



EXPERIMENTAL MODAL ANALYSIS OF A ROTATING ROTOR

Lappeenranta–Lahti University of Technology LUT
Master's Degree in Mechanical Engineering, Master's Thesis
2021

Hari Pathak

Examiner(s): Professor, Jussi Sopenen

Dr, Neda Neisi D.Sc. (Tech.)

ABSTRACT

Lappeenranta–Lahti University of Technology LUT

LUT School of Energy Systems

Mechanical Engineering

Hari Pathak

Experimental modal analysis of a rotating rotor

Master's thesis

2021

58 pages, 32 figures, 8 tables and 1 appendix

Examiner(s): Professor Jussi Sopanen and Neda Neisi D.Sc. (Tech.)

Keywords: Experimental modal analysis, Frequency, Mode shapes, damping ratio, Rotor, FRF, Impact hammer, Excitation, Scanning Vibrometer, Rotordynamics, FEM.

Rotordynamics analysis of a rotating machine is a fundamental process to understand the vibration characteristics of a rotating components as it ensures the proper functioning of the machine. Improper vibration in the machine may cause excessive noise, or even damage the components in the rotating machines. For smooth operation of the rotor system in machines have been studied through Finite element method (FEM), experimental modal analysis (EMA) and operational modal analysis (OMA) over the years.

EMA of rotating machines is a method for obtaining the natural frequencies, mode shapes and damping ratios to evaluate critical speeds and resonances from the measurement. EMA for stationary rotors have been established to some accuracy in the past, however, for rotating rotor case, the modal parameters like frequencies, mode shapes and damping ratios are difficult to extract from the measurement. The reason for this difficulty is the rotating machines having additional lateral and tangential forces along with gyroscopic moments in rotating components. The objectives of this thesis were to obtain the modal parameters of rotating rotor.

The frequencies, mode shapes and damping ratio were established through measurement. In this study the experimental modal analysis is done on the laboratory setup. The main frequencies are compared with for the rotor at stand still and rotating rotor. The measurement was done with 1) accelerometer sensor and impact hammer and 2) scanning vibrometer with automated hammer. Damping ratio was calculated using half power method. The results were compared and found that the obtained modes and frequencies agreed in both cases of measurement to each other.

ACKNOWLEDGEMENTS

I sincerely thank my supervisors Professor Jussi Sopanen, Dr. Neda Neisi, and Dr. Eerik Sikanen for providing me with the opportunity to work on this thesis. Dr. Neisi was a great help for me in understanding the topic and execution of this thesis. Dr. Sikanen provided me with the valuable information regarding the test rig. I would like to thank my parents, Nityananda Pathak and Anita Pathak, my brother Dr. Budhi Pathak for his council. My wife Manisha, who is always supporting. All my teachers, Thank You.

SYMBOLS AND ABBREVIATIONS

Roman Alphabets

| | |
|----------------------|--|
| A | Complex vector in eigenvalue problem |
| B | Complex vector in eigenvalue problem |
| C | Global Damping Matrix |
| C_{YY} | Damping in Y-coordinate in Ns/m |
| C_{ZZ} | Damping in Z-coordinate in Ns/m |
| E | Modulus of Elasticity |
| e_{ub} | Eccentricity of the unbalance |
| F | Externally Applied Force |
| f | frequency in per second or Hertz |
| G | Gyroscopic Matrix |
| $H(f)$ | Frequency response function represented in Hertz |
| $H(\omega)$ | Frequency response function represented in radians per second |
| j | Imaginary number |
| J_{xx} | Moment of Inertia in xx-coordinate |
| J_{yy} | Moment of Inertia in yy-coordinate |
| J_{zz} | Moment of Inertia in zz-coordinate |
| K | Global Stiffness Matrix |
| $\tilde{\mathbf{K}}$ | The normalized stiffness matrix |
| k_s | Shear correction factor |
| K_{YY} | Stiffness in Y-coordinate in N/m |
| K_{ZZ} | Stiffness in Z-coordinate in N/m |
| M | Mass Matrix |
| \mathbf{M}^{-1} | Inverse of mass matrix |
| m_{ub} | Unbalance mass |
| n | Number of degree of freedoms |
| Q₁ | Unbalance force vectors related to the constant speed of the rotor |

| | |
|---------------------|--|
| \mathbf{Q}_2 | Unbalance force vectors related to the variable speed of the rotor |
| \mathbf{q} | Nodal displacement vector |
| $\dot{\mathbf{q}}$ | Nodal velocity vector |
| $\ddot{\mathbf{q}}$ | Nodal acceleration vector |
| \mathbf{q}_n^c | Unbalance vectors at constant speed of rotor |
| \mathbf{q}_n^{nc} | Unbalance vectors at variable speed of rotor |
| r | Modal coordinate system |
| s | Complex scalar in eigenvalue problem |
| \mathbf{u} | Real displacement vector |
| \mathbf{v} | Eigenvectors $n \times 1$ |
| v_z | Vibration velocity of a point in z-direction |
| V_{an} | Fourier coefficients for complex mode shape components |
| V_{bn} | Fourier coefficients for complex mode shape components |

Greek Alphabets

| | |
|------------|---|
| ρ | Material density in kg/m^3 |
| ν | Poisson's ratio |
| Ω | Angular velocity of the rotor |
| α | phase angle |
| ω | frequency in radians per seconds |
| ω_1 | Sideband Frequency on the left of natural frequency after half power |
| ω_2 | Sideband Frequency on the right of the natural frequency after half power |
| ω_n | Natural frequency |
| ξ | Damping ratio |
| λ | Eigenvalues (n quantities) |
| δ | Logarithmic decrement |

Abbreviations

| | |
|---------|-----------------------------------|
| AMB | Active Magnetic Bearing |
| BW | Backward Whirling Mode |
| DE | Drive End |
| DOF | Degree of Freedom |
| EMA | Experimental Modal Analysis |
| FEM | Finite Element Method |
| FFT | Fast Fourier Transform |
| FRF | Frequency Response Function |
| FW | Forward whirling Mode |
| LTI | Linear Time Invariant |
| MDOF | Multi Degree of Freedom |
| NDE | Non-Drive End |
| OMA | Operational Modal Analysis |
| RoBeDyn | Rotor Bearing Dynamics |
| SLDV | Scanning Laser Doppler Vibrometer |

Table of contents

Abstract

Acknowledgements

Symbols and abbreviations

| | |
|---|----|
| 1. Introduction | 9 |
| 1.1 Background | 9 |
| 1.2 Research Problems | 13 |
| 1.3 Objectives of the thesis and Scope..... | 13 |
| 1.4 Structure of the thesis..... | 14 |
| 2. Rotordynamics Analysis Theory | 15 |
| 2.1 Rotordynamics | 15 |
| 2.2 Equation of Motion | 15 |
| 2.3 Frequency Response Function | 19 |
| 2.3.1 Fast Fourier Transform (FFT)..... | 21 |
| 2.3.2 Spectral Leakage and Use of Windows | 22 |
| 2.4 Impact Hammer Method of Excitation | 25 |
| 2.5 Scanning Laser Doppler Vibrometer | 26 |
| 2.6 Damping Ratios Using Half Power Method | 27 |
| 2.7 Damping Ratio Using Logarithmic Decrement Method..... | 28 |
| 2.8 Numerical Simulation using MATLAB RoBeDyn Toolbox | 30 |
| 2.8.1 Campbell Diagram | 30 |
| 3. Measurement | 32 |
| 3.1 Electric Motor | 33 |
| 3.2 Bearings, Shaft and Discs | 33 |
| 3.3 Measurement Sensors..... | 34 |
| 3.4 Measurement Set-up..... | 36 |

| | |
|--|----|
| 4. Results and Discussion | 38 |
| 4.1 RoBeDyn Simulation Results | 38 |
| 4.2 The Campbell diagram and Unbalance Response..... | 39 |
| 4.3 Case Study of Standstill Rotor with Impact Hammer and Acceleration Sensor...42 | |
| 4.4 Case Study of Rotating Rotor and Measurement with Accelerometer Sensor | 46 |
| 4.5 Case Study of Standstill Rotor with Scanning Vibrometer..... | 49 |
| 4.6 Summary of the Obtained Results..... | 51 |
| 5. Conclusions | 53 |
| References..... | 55 |

Appendices

Appendix1. The damping ratio extraction methods relationship.

1. Introduction

Large number of industries such as oil and gas, aviation, steel manufacturing industries, energy production, paper industries, ship building industries, are using rotating machines. The rotating machineries consists of different components like rotor, bearings, shafts, couplings. The rotordynamics analysis is the most important procedure for design of rotating machines. The vibration characteristics of rotating components is important for the proper functioning of a machine during the optimal operational speed. The high vibration may cause excessive noise or even damage the components in the rotating structures. There have been several studies conducted for the smooth operation of rotor systems since its inception. Finite Element Method (FEM), Experimental Modal Analysis (EMA), Operational Modal Analysis (OMA) are some of the methods to obtain the modal characteristics like natural frequencies, damping ratios and mode shapes. The modal parameters obtained can be used to evaluate the rotor critical speeds and resonances.

1.1 Background

Experimental modal analysis is the method where the structure is defined in terms of it inherit dynamic properties like frequencies, mode shapes, and damping factors (Avitabile 2001). The experimental modal analysis of a stationary rotors, which has been established to certain accuracy, whereas the study of rotating rotors has some fundamental differences because of the rotation. The main difference is the lateral forces and moments developed due to the spin of the rotors (Friswell et al. 2010, Pp. 1-3). Obtaining modal parameters become challenging in case of rotating rotors because of the additional forces developed due to the gyroscopic effect, tangential forces due to simultaneous spin and whirl, and non-self-adjoint nature of a rotating structures where principles of reciprocity become invalid (Chouksey, Dutt & Modak 2012). This implies that, in rotating rotors, the system matrix to compute eigenvectors (right eigenvectors) are different from those computed from system matrix's transpose (left eigenvectors). Therefore, the modal model has eigenvalue, which is associated with the natural frequencies of the rotor, and both right eigenvectors, and left eigenvectors, which are associated with the mode shapes are needed to fully understand the dynamic behavior of the rotor system. (Bucher & Ewins 2001.) The forward and backward

modes are associated with this non-self-adjoint phenomena or reciprocity principles invalidity of the rotating rotors unlike non-rotating structures.

In the review article, modal analysis and testing of rotating structures, Bucher and Ewins (2001) have presented different methods of experimental modal analysis for the rotating structures. The forward and backward modes are effectively presented for the modal parameter like frequencies, mode shapes, and damping ratios identification by (Lee 1991; Lee & Joh 1993) in complex modal testing for rotating machines. There are several ways of exciting the structures in modal analysis. The use of impulse hammer to excite the rotors were used by (Nordmann 1984; Chouksey et al. 2012; Jalali et al. 2014). The measurement was done using a displacement sensor (Nordmann 1984; Chouksey et al. 2012) and acceleration sensor were used by Jalali et al. (2014).

In figure 1, the measurement method used by Nordmann (1984) is presented. The impact hammer is used to excite the system and sensor takes the measurement (middle), the time domain response is shown in top left and top right. The FRF after Fast Fourier Transform (FFT) is shown in the bottom left and bottom right of the figure. The rotor disc at the middle is supported by two bearings at the two ends of the rotor, is excited using an impact hammer at a location in the rotor and the measurement is taken from the displacement sensor at different locations in the rotor. The measurement was also possible by measuring the excited frequencies by a sensor at a point in a rotor and the impact hammer excitation at different locations in the rotor. (Nordmann 1984.) The hammer method of excitation is simple to use, the appropriate selection of hammer is enough to excite the broadband of modes and frequencies. Hammer excitation also has some limitations such as the magnitude and direction of force are not readily reproducible. It is possible for uncontrolled tangential components to exist and as a wideband excitation, it has low signal-to-noise ratio. (Bucher & Ewins 2001.)

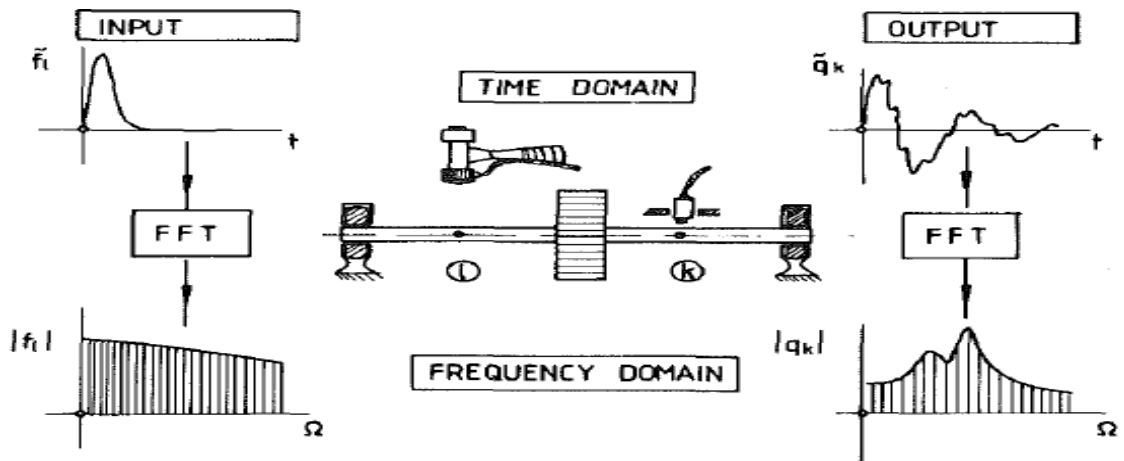


Figure 1. The measurement of the frequency response functions (Nordmann 1984).

Another way of excitation is the shaker excitation. The shaker can be connected to the shaft through low friction bearings (Bucher & Ewins 2001). This kind of excitation was used by placing vertical and horizontal shakers for estimating the FRF (Peeters, et al. 2001; Cavalca, Cavalcante, & Okabe 2005; Idehara & Junior 2020) also applied the shaker-based excitation. The figure 2 shows the shaker based excitation method. There are some advantages considering the use of shaker excitation which is, the typical signal generator can adjust the amplitude and frequency of the force. It is also possible to produce forward and backward rotational forces and get an excellent signal-to-noise ratio. However, disadvantage related to shaker exciter is that it needs special attachment to the shaft and thereby, the shaft motion could significantly affect the applied forces. (Bucher & Ewins 2001.)

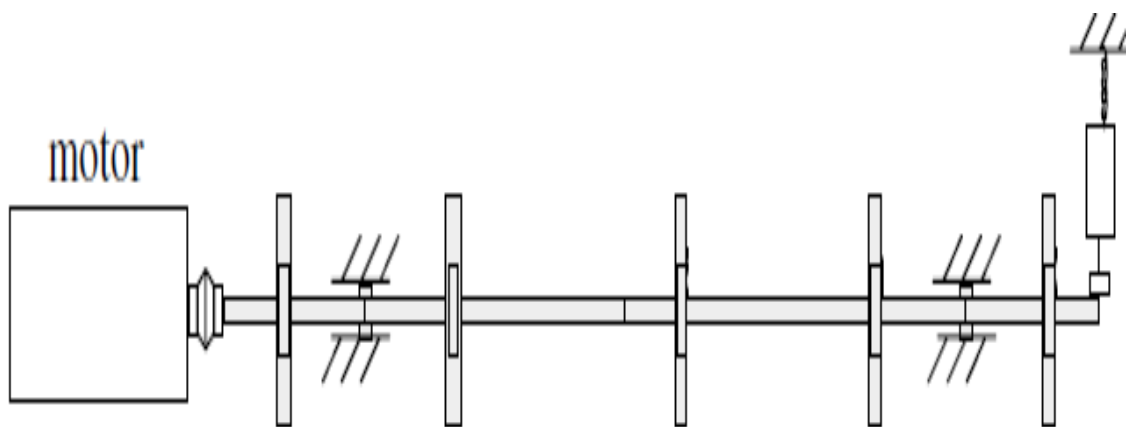


Figure 2. The schematic representation of shaker based excitation where the shaker is placed at the free end of the rotor (Bucher & Ewins 2001).

Active magnetic bearing excitation method has been increasing since the turn of this century. The use of Active Magnetic Bearing (AMB) for exciting the rotating structures was applied by Kreuzinger-Janik and Irretier (2000), in a study conducted to identify the unbalance estimation by means of experimental modal analysis. They applied a non-contact magnetic exciter system, and the magnetic exciter was driven by harmonic current which induced a double frequency harmonic force on the rotor (Kreuzinger-Janik & Irretier 2000). The figure 3 shows the active magnetic bearing type excitation. AMB can considerably reduce the workload to create a controlled excitation and multiple forces could be applied for example, two forces per bearing, to give multiple input in the experimental setup (Bucher & Ewins 2001).

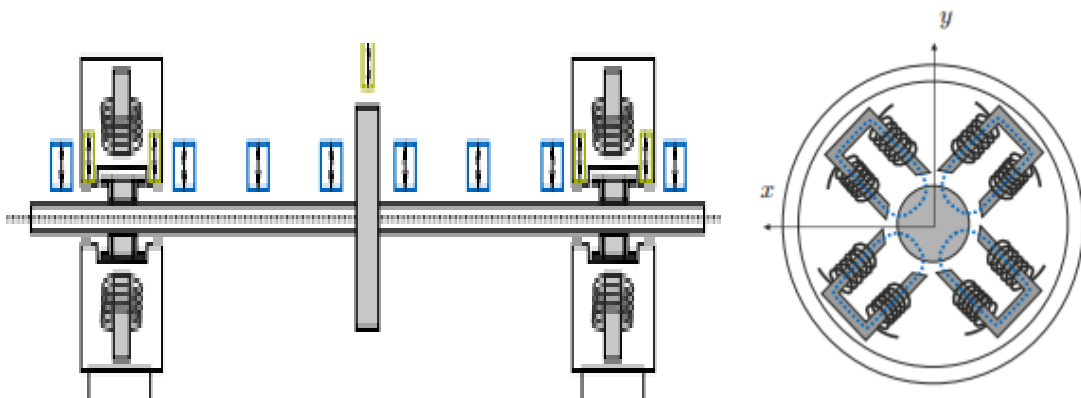


Figure 3. The active magnetic bearing excitation used in a rotor system (left) and conceptual AMB exciter (right) (Maierhofer et al. 2019).

The problem associated with AMB based excitation is the size and difficulty caused by movement of the shaft in the magnetic region.

There is also possibility of vibration analysis in the operational condition of the rotors. The Operational Modal Analysis (OMA) is used in such cases. The natural vibrations of the structures are used instead of external excitation. The vibration properties can be identified by the measured output signals. However, the need for structure to be Linear Time Invariant (LTI), and all the frequencies must be excited evenly to get white noise in the frequency range for the forces acting, it is difficult to achieve LTI and white noise if several

components move in relation to one another. (Lorenzo 2017, Pp. 2-3.) This method can be especially important in prediction of the machine conditioning and predictive maintenance of the rotating machines.

1.2 Research Problems

The basis for this thesis is to validate the modal parameters obtained from experimental modal analysis of a rotating rotor and compare it to the numerical simulation. The simulated numerical method could be carried out from the existing rotor bearing dynamics program developed at machine dynamics laboratory in LUT University (RoBeDyn software) available in MATLAB environment. This research intends to answer the following questions.

- How to conduct the modal analysis of a rotating rotor?
- What are the modal parameters measured from vibration data of the EMA of rotating rotor?
- What is the best way of obtaining modal parameters based on the existing literature study for rotating rotor?
- Does the result obtained match with different methods applied and does those result match with the simulated results obtained?

1.3 Objectives of the thesis and Scope

The first and foremost objectives of this thesis is to find answers to the research questions. The aim of this thesis is to carry out the experimental modal analysis of a rotating rotor in the laboratory environment and obtain modal characteristics like frequencies, damping ratios, and mode shapes of the rotor system. The obtained result from the experiment will then be compared with the numerical simulation-based model in RoBeDyn software in the MATLAB environment. The experimental work needs to be conducted in the Machine Dynamics Laboratory at LUT University.

The scope of this thesis is limited to obtaining the modal parameters on a laboratory set up presented in this thesis. Electric motor run rotor system and analyzing the obtained results

compare it with the RoBeDyn obtained results with different excitation processes. The thesis only considers the specific setup model and limited to the obtained value for the set up. Measurement results are obtained using an accelerometer sensor on the horizontal position, which could also be vertically placed, and thus, the parameters might not sufficiently present the idea of the rotating rotor overall vibration modes. Scanning Vibrometer has been applied to the stationary rotor and damping ratio is obtained through the half power method. The analysis is mainly conducted to get the time domain and converting it to frequency domain spectrum analysis. RoBeDyn based numerical simulation is limited mainly to the Campbell diagram to analyze the critical frequency of the system for the comparison of the measured frequency response from the experimental work.

1.4 Structure of the thesis

The chapter 1 of the thesis is the introduction section where, the background of rotordynamics is explained. Research objectives and scope are also presented in this chapter. In chapter 2, the methods section has been presented. Chapter 3 provides the measurement methods and equipment for the thesis. Chapter 4 is the section for results of measurements and numerical simulation and comparison of the results and discussions. The chapter 5 deals with the conclusion.

2. Rotordynamics Analysis Theory

This section of the thesis explains about the methods used. The methods are based on literature studies on rotordynamics and are basis for the experimental and numerical simulation approach presented to get the modal characteristics of a rotor system.

2.1 Rotordynamics

A rotor vibrates in an axial, torsional, and lateral directions. Axial vibration occurs along the rotor axis whereas torsional vibration twists the rotor about its rotation axis. Meanwhile, the rotor is displaced horizontally and vertically by the lateral vibrations in case of horizontal rotors. The lateral vibrations are caused by the lateral forces like unbalance forces. All these vibration combines to create the orbital movement of the rotor in a plane perpendicular to its rotation axis. The analysis is determined by the type of rotor if it is rigid or flexible, the type of bearings used, and the support structure of the rotor. (Friswell et al. 2010, Pp. 5-7.) The development of Finite Element Method (FEM) and its commercialization has helped predict the rotordynamics analysis to greater accuracy. Rotordynamics analysis is important because of the need for high-speed machine development as speed in rotating machines means higher production, and operating machines in higher temperatures as the temperatures increases the thermal stress increases which results in lowering of damping and stiffness in rotating machines thus increasing the vibration problem. Rotor dynamics is not only important in design phase but, also during the machine's operation and predictive maintenance phase. The vibration spectrum study provides information about the potential problems that may occur leading to the component's failure and thus prevents such problems from occurring, in time. (Genta 2005, Pp. 1-4.)

2.2 Equation of Motion

The rotating machines may have several parts such as rotor, shafts, discs, bearing, and other supporting parts. The equation of motion for any damped multi degree of freedom (MDOF) system with n degree of freedom can be written as following equation.

$$\mathbf{M}\ddot{\mathbf{q}} + \mathbf{C}\dot{\mathbf{q}} + \mathbf{K}\mathbf{q} = \mathbf{F} \quad (1)$$

\mathbf{M} , \mathbf{C} and \mathbf{K} in the equation 1 are mass matrix, damping matrix and stiffness matrix respectively with $n \times n$ sizes, where, n is number of degree of freedoms (DOF), \mathbf{q} is generalized coordinate and generalized force is denoted by \mathbf{F} . Free Vibration can be calculated by assuming the generalized force vector to zero ($\mathbf{F}=\mathbf{0}$) and the undamped vibration is when the damping is assumed to be zero ($\mathbf{C}=\mathbf{0}$). (Friswell et al. 2010, p. 34.)

For undamped vibration the equation of motion becomes

$$\mathbf{M}\ddot{\mathbf{q}} + \mathbf{K}\mathbf{q} = \mathbf{0} \quad (2)$$

Assuming the solution in the form,

$$\mathbf{q}(t) = \mathbf{u}e^{j\omega t} \quad (3)$$

where \mathbf{u} is a real vector, j is imaginary number, and ω_n is natural frequency of MDOF system and is real and positive. The exponential terms in equation 3 represents harmonic motion (Inman 2014, p. 309-310) and is represented by

$$e^{j\omega t} = \cos \omega t + j \sin \omega t \quad (4)$$

The equation 3 after double integration forms,

$$\ddot{\mathbf{q}}(t) = \omega^2 \mathbf{u}e^{j\omega t} \quad (5)$$

Since, exponential term cannot be zero, using this information in equation 2 gives following equation. (Inman 2014, p. 309-310.)

$$\omega_n^2 \mathbf{M} \mathbf{u} = \mathbf{K} \mathbf{u} \quad (6)$$

The equation 6 is generalized eigenvalue problem. The natural frequencies can be computed and the sign errors occurring in the computation of natural frequency could be avoided from the equation 4. For each value of ω^2 the vector \mathbf{u} satisfies the equation 4. Hence, for n numbers of eigenvalues ω^2 , there are n numbers of eigenvectors can be computed. The eigenvalue and eigenvectors could also be computed from the symmetric eigenvalue problem to get the natural frequencies and modes shapes. (Inman 2014, p. 309-310.)

$$\omega^2 \mathbf{v} = \mathbf{M}^{-\frac{1}{2}} \mathbf{K} \mathbf{M}^{-\frac{1}{2}} \mathbf{v} \quad (7)$$

The normalized stiffness matrix $\tilde{\mathbf{K}}$ can be formed from equation 7 and symmetric eigenvalue problem can be solved such that $\tilde{\mathbf{K}} \mathbf{v} = \lambda_i \mathbf{v}_i$ and $\lambda_i = \omega_i^2$ the vector \mathbf{v}_i is called normalized eigenvector (Inman 2014, p. 318-321).

For the solution of eigenvalues and eigenvectors of a free damped systems, the equation of motion becomes,

$$\mathbf{M} \ddot{\mathbf{q}} + \mathbf{C} \dot{\mathbf{q}} + \mathbf{K} \mathbf{q} = \mathbf{0} \quad (8)$$

The eigenvalue problem is given by following equation which can be obtained from the transient solution (Friswell et al. 2010, p. 39-40).

$$[s\mathbf{A} + \mathbf{B}] \mathbf{v} = \mathbf{0} \quad (9)$$

In equation 9 s is a complex scalar, \mathbf{v} is a complex vector and \mathbf{A} , and \mathbf{B} are matrices. This eigenvalue problem has $2n$ solutions and occurs in complex conjugate pairs s_i and s_{n+i} . The complex conjugate pairs are defined by following equation. (Friswell et al. 2010, p. 39-40.)

$$s_i, s_{n+i} = \omega_i \left(-\xi_i \pm \sqrt{\xi_i^2 - 1} \right) \quad (10)$$

In equation 10 ω_i and ξ_i are natural frequency and damping ratio of the i th mode. The underdamped system's eigenvalues where $\xi_i < 1$, the equation 11 below is shown. (Friswell et al. 2010, p. 40.)

$$s_i, s_{n+i} = \omega_i \left(-\xi_i \pm \sqrt{1 - \xi_i^2} \right) = -\xi_i \omega_i \pm j \omega_{di} \quad (11)$$

The eigenvectors corresponding to the eigenvalues are also in complex conjugate pairs, $\mathbf{v}_{n+i} = \mathbf{v}_i$. \mathbf{v}_i are complex constants depending upon initial displacement and velocity (Friswell et al. 2010, p. 40).

One of the most prevalent sources of vibration in rotating machines is due to the unbalance (Ahmed & Nandi 2020, p. 21). There are several reasons for the unbalance in the rotor system. The unbalance could be due to the uneven distribution of mass, dirt, eccentricity of the mass, etc. The eccentricity of the mass is one of the main causes for the unbalance forces, and the discs needs to be mounted perpendicular to the rotational axis but when it is mounted obliquely, the unbalance moment is caused (Krämer 1993, p. 52). The unbalance forces and rotational speed dependent terms in the rotordynamics are added in the equations to address the equation of motion. The equation of motion for variable rotational speed in case of rotordynamics can be written as following equations 12. (Kärkkäinen 2007, p. 30-31.)

$$\mathbf{M}\ddot{\mathbf{q}} + (\mathbf{C} + \Omega\mathbf{G})\dot{\mathbf{q}} + \left(\mathbf{K} + \frac{1}{2}\dot{\Omega}\mathbf{G} \right) \mathbf{q} = \Omega^2\mathbf{Q}_1 + \dot{\Omega}\mathbf{Q}_2 + \mathbf{F} \quad (12)$$

In equation 12, Ω is the rotational speed of the rotor, the gyroscopic matrix is represented by \mathbf{G} , which is a skew symmetric matrix and is derived from the kinetic energy because of the gyroscopic moments, \mathbf{F} represents the vector of external force applied, \mathbf{q} is the nodal coordinate vector. \mathbf{Q}_1 and \mathbf{Q}_2 are the unbalance force vectors of the rotor and are related to the constant and variable speed of the rotor respectively. (Kärkkäinen 2007, p. 30-31.)

$$\mathbf{Q}_1 = \begin{bmatrix} \mathbf{q}_1^c \\ \mathbf{q}_2^c \\ \vdots \\ \mathbf{q}_n^c \end{bmatrix} \quad \mathbf{Q}_2 = \begin{bmatrix} \mathbf{q}_1^{nc} \\ \mathbf{q}_2^{nc} \\ \vdots \\ \mathbf{q}_n^{nc} \end{bmatrix} \quad (13)$$

In equation 13, n is the number of nodes, \mathbf{q}_n^c and \mathbf{q}_n^{nc} are the unbalance vectors at constant and variable speeds. The unbalance vectors for i^{th} node at time t can be represented as the following equation. (Kärkkäinen 2007, p. 30-31.)

$$\mathbf{q}_i^c = \begin{bmatrix} m_{ub}e_{ub} \cos(\Omega t + \alpha) \\ m_{ub}e_{ub} \sin(\Omega t + \alpha) \\ 0 \\ 0 \end{bmatrix} \quad \mathbf{q}_i^{nc} = \begin{bmatrix} m_{ub}e_{ub} \sin(\Omega t + \alpha) \\ -m_{ub}e_{ub} \cos(\Omega t + \alpha) \\ 0 \\ 0 \end{bmatrix} \quad (14)$$

In equation 14, α is unbalance phase angle, m_{ub} is mass of the unbalance of i^{th} node and e_{ub} is eccentricity of the unbalance of i^{th} node. (Kärkkäinen 2007, p. 30-31)

2.3 Frequency Response Function

The Frequency response function (FRF) commonly referred as $H(\omega)$, if represented in radians per second (rad/s) or $H(f)$, if represented in hertz (Hz) is the ratio of system's steady-state response to an applied sinusoidal input, like force, compelled displacement. The FRF is typically expressed in complex form, it can also be represented in amplitude or phase form. The sinusoidal input begins at $-\infty$ and before the transient response dies in computing the FRF. This results in the response output also becomes sinusoidal. Normal mode summation method can be used to calculate the FRFs of the multiple DOF systems where FRF is sum of many single DOF systems. (Thorby 2008, p. 286.)

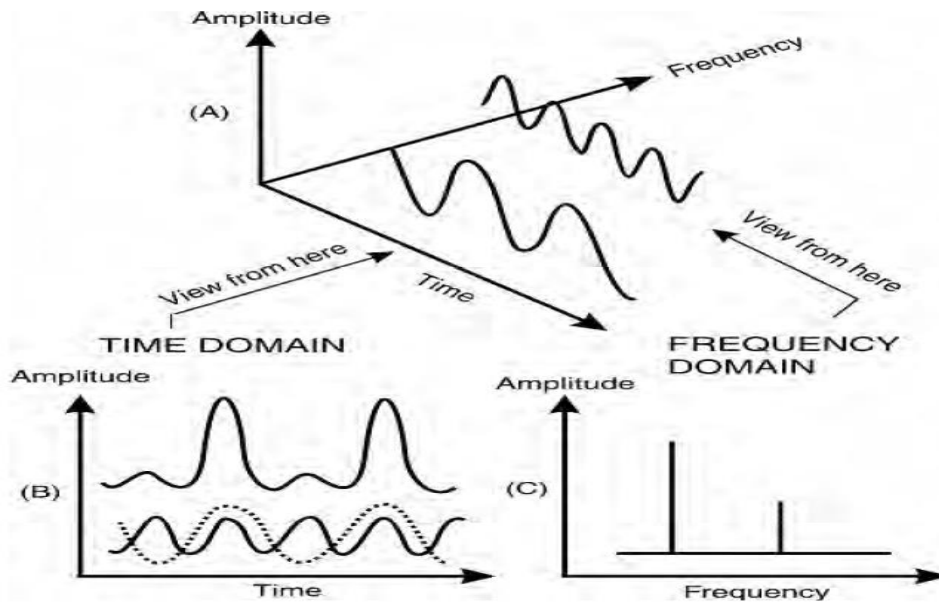


Figure 4. The FFT (Scheffer & Girdhar 2004, p. 56). (A) on top shows the viewing angle for the different frequencies of a system, (B) on left bottom is time domain response and (C) on bottom right shows the frequencies after FFT.

The Laplace transform ($H(s)$) of the output response to the input driving force for harmonic force applied to equation of motion is represented by following equation (Inman 2014, p. 148-149)

$$H(s) = \frac{1}{(ms^2 + cs + k)} \quad (15)$$

In equation 15, s is the transform variable which is a complex number. If we consider $s=j\omega$, the equation becomes,

$$H(j\omega) = \frac{1}{k - m\omega^2 + c\omega j} \quad (16)$$

The equation 16, $H(j\omega)$ is called frequency response function (FRF). FRF is therefore the transfer function of the system calculated in $s=j\omega$. (Inman 2014, p. 148-149.)

It is possible to depict system response or vibration by measuring displacement, velocity, and acceleration amplitudes over time and frequency domain. The amplitude changes with the time in the time domain while, the amplitudes are represented in frequency in the

frequency domain. The response can be studied in either time domain or frequency domain. The conversion of time domain signals to the frequency domain signals can be achieved by the Fast Fourier Transform (FFT). Figure 4 shows the FFT. (Scheffer & Girdhar 2004, p. 56.) Leakage is one of the major problems causing distortion of data associated with the transformation of time domain data to the frequency domain. Leakage can be reduced by applying weighting functions also known as windows. The linear spectra from FFT data are then averaged to power spectrum such as input power spectrum, output power spectrum, and cross power spectrum. After this, the modal data such as system frequency, damping can be extracted from FRF. Mode shapes can be obtained from collection of FRFs. The averaged spectrum also contains coherence functions, which informs about the relativity of the output signal to the measured input signal. (Avitabile 2001.)

2.3.1 Fast Fourier Transform (FFT)

The time domain signals conversion to frequency domain signals with reduction in complexity from Discrete Fourier Transform (DFT) is achieved by an efficient algorithm known as Fast Fourier Transform (FFT). $N \log_2 N$ is used instead of N^2 as in case of DFT to compute the complex multiplications of the signal length N . Another benefit is the phase information of the signal is retained by FFT for inverse transformation possibility. (Ahmed & Nandi 2020, p. 67.) The misrepresentation of the analog signal by digital recorder when converting the signals from Analog to Digital (A/D) converter (Inman, 2014, p. 581). Avoiding aliasing to avoid lower frequency appearance than the actual signal is important criteria for FFT, for this, the Nyquist criterion could be used. The sampling frequency, F_s as suggested by Nyquist criterion needs to be at least double the maximum frequency component of the signal.

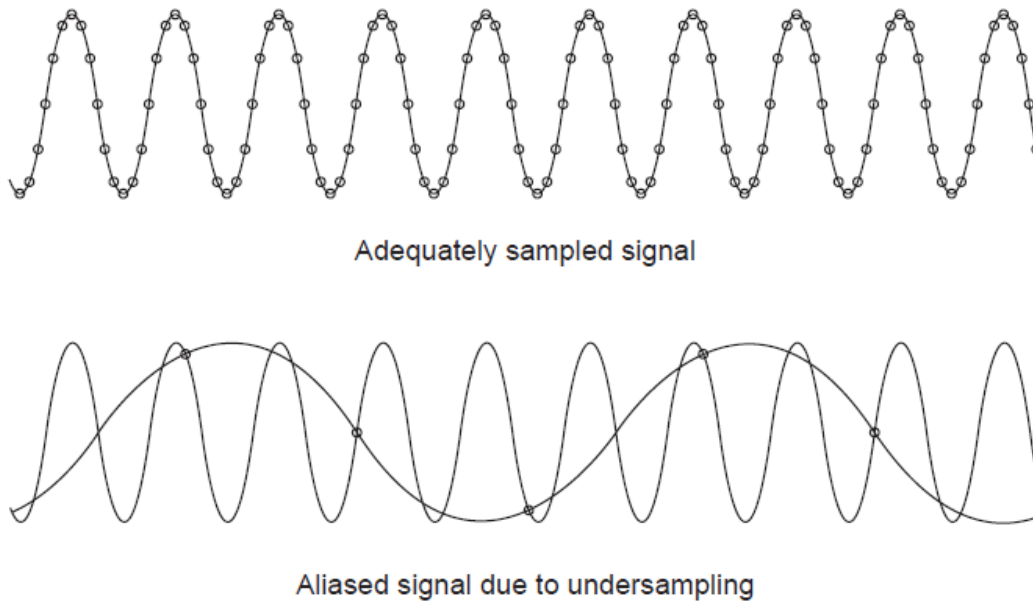


Figure 5. Aliasing due to the under sampling of signals (Cerna & Harvey 2000).

The figure 5 shows the aliasing due to under sampling. The antialiasing filters could be used to prevent the aliasing before the signal is digitized. (Cerna & Harvey 2000.)

2.3.2 Spectral Leakage and Use of Windows

From the time domain analysis, the time of length T converted by FFT, is assumed to be sinusoidal with harmonic frequencies $1/T, 2/T, 3/T, \dots$ and so on. In cases where waveform is periodic T can be selected such that T equals the period perfectly. However, it is not possible in case of random data and the resultant harmonic frequencies produces output in adjacent frequencies and thus this situation is called leakage. The figure below shows the spectral accuracy and leakage. In figure 6, (a) is the spectrum over the time T and (b) is the output frequency in FFT. We see that there is no leakage, and a single line in the frequency domain is present but in case of (c) in the figure, we see that the time T is incomplete sinusoidal wave, and the resultant output frequency (d) has several lines showing the leakage. (Thorby 2008, p. 318.) To prevent this leakage, window can be used.

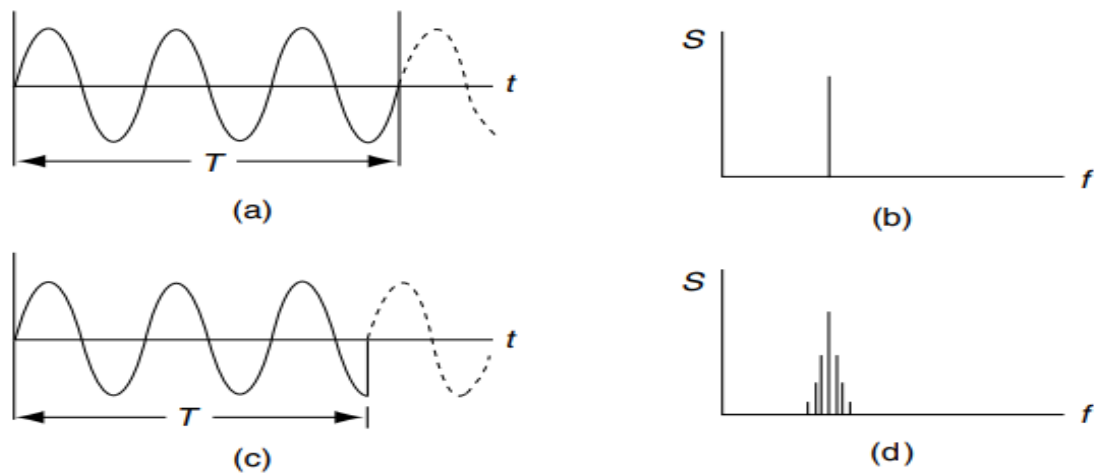


Figure 6. The spectral accuracy and leakage (Thorby 2008, p. 318).

Windows can be used to reduce the spectral leakage. The waveform of the sampling fixed time intervals gets truncated at the start and end of the analog signal captured. The discontinuities are the result of this in the continuous waveform. The windows forces zero at the start and the end of the sample period of the discontinuity data to make it continuous. The figure 7 shows the effect of windowing on a sine wave. (Gerhard 2003.)

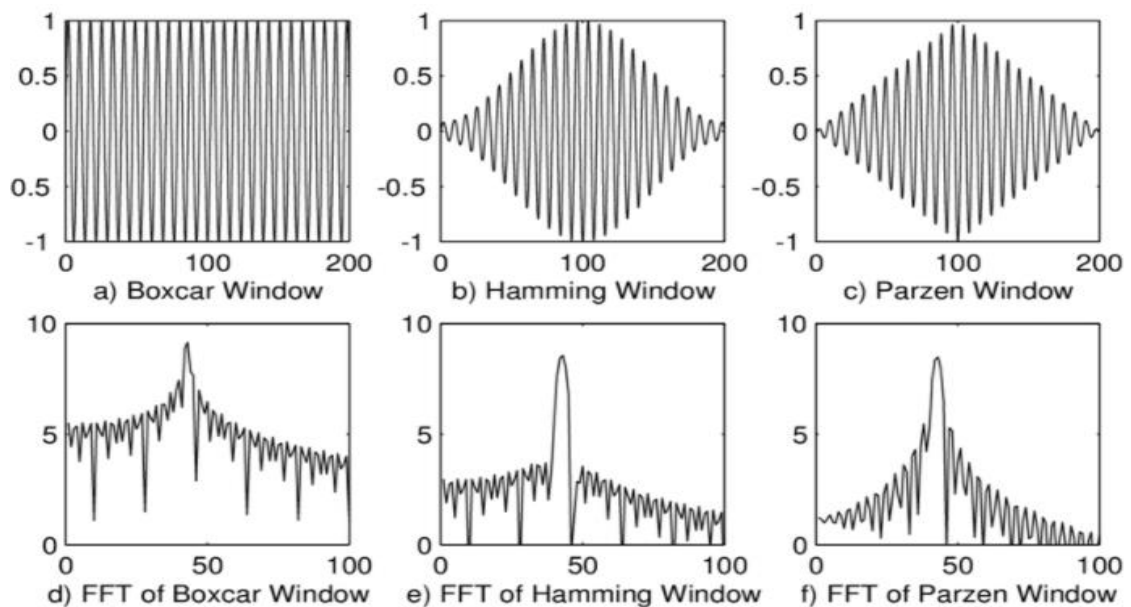


Figure 7. The effect of different windowing on a sine wave (Gerhard 2003).

The accuracy in amplitude is also possible in closely spaced frequencies by using windows. No-window (Rectangular), Hanning or Hann, Hamming, Flat-top are some of the windows

used (Scheffer & Girdhar 2004, p. 59). The table 1 below shows the choice of the window based on the signal (Cerna & Harvey 2000).

Table 1. Choice of window based on the signal (Cerna & Harvey 2000).

| Signal Content | Window |
|---|------------------|
| Sine wave or combination of sine waves | Hann |
| Sine wave (amplitude accuracy is important) | Flat Top |
| Narrowband random signal (vibration data) | Hann |
| Broadband random (white noise) | Uniform |
| Closely spaced sine waves | Uniform, Hamming |
| Excitation signals (Hammer blow) | Force |
| Response signals | Exponential |
| Unknown content | Hann |

The figure 8 shows the use of Hanning window to reduce the leakage.

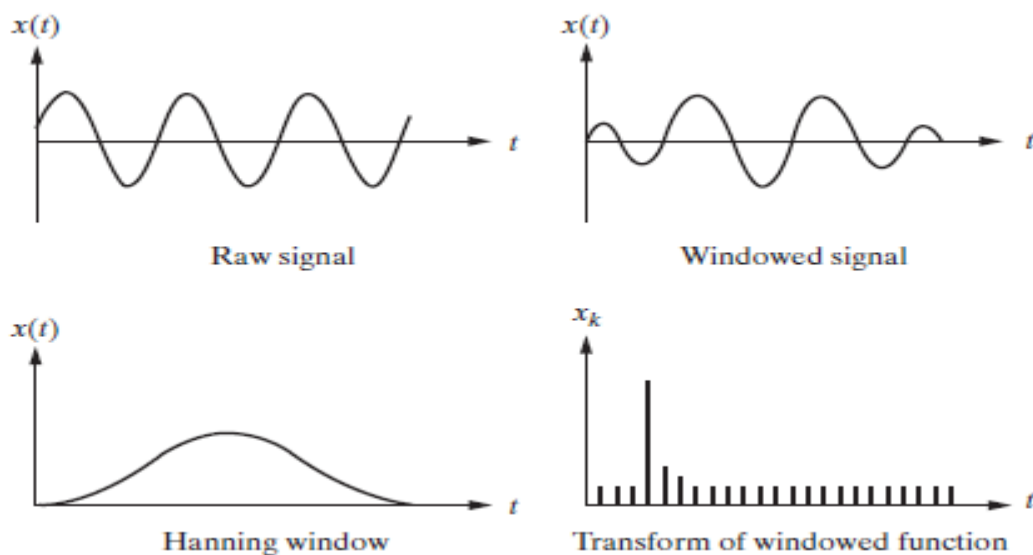


Figure 8. The application of Hanning window function to avoid the spectral leakage (Inman 2014, p. 584).

In figure 8, the Hanning window on the bottom left is applied to the raw signal on the top left and windowed signal on the top right is achieved which is computed in FFT to get the frequency domain results (Inman 2014, p. 584). In total, 95% of the cases Hanning window

can be used. However, analyzing the transient signal like using impact or resonance signals, the use of force or exponential windows are preferable compared to the spectral windows as the force window removes the stray signals at the end. (Cerna & Harvey 2000.)

2.4 Impact Hammer Method of Excitation

Impact hammer modal testing is a fast way of exciting a wide range of frequency. Most important aspects to carry out impact testing are the selection of hammer and the use of exponential windowing for response transducers. Exponential decay windowing prevents the leakage, however, selecting narrow bandwidth for measurements and increasing spectral lines of resolution during impact measurements could avoid the leakage and prevent the use of windowing. (Avitabile 2001.) Hammer testing can be subjected to roving (moving hammer to different locations for measurement) hammer method, roving (moving sensor to different locations for measurement) accelerometer measurement or applying multiple transducers for measurements. All modes of the structure need to be excited by the hammer selected, as the top frequency limit induced by the hammer reduces as the hammerhead mass is raised, and it is increased if the stiffness of the hammer tip is increased (Inman 2014, p. 577-578). In case of this thesis, the roving accelerometers with manual impact hammer in a fixed point is used and the scanning vibrometer is used with the automated hammer. The table 2 below shows the hammer size used for different applications.

Table 2. Range of Hammer used for different purpose (Bruel & Kjaer 2003).

| Hammer Size in Pound (<i>lb</i>) | Application |
|---|---|
| Sledgehammer, 12 | Building and Bridges |
| Hand Sledge, 3 | Large Shafts, and larger machine tools |
| Hammer, 1 | Car framed machine tools |
| General Purpose, 0.3 | Components |
| Mini Hammer, less than 0.3 | Hard drives, Circuit boards, turbine blades |

The magnitude and the pulse duration for impact testing depend upon the weight of hammer, hammer tip (steel, plastic, rubber), inherit dynamic properties of the surface and velocity of

impact. The impact hammer can be used for field work because of no fixturing needed, the speed and portability, however, the high crest factors in case of impact hammer could lead the structure into non-linear behavior. (Bruel & Kjaer 2003.)

2.5 Scanning Laser Doppler Vibrometer

The scanning Laser Doppler Vibrometer (SLDV) works by the principle of Doppler effect where the velocity at a point is measured by a focused laser beam using the doppler shift between the incident ray and scattered ray. The measurement can be done such that the beam is continuously swept over the vibrating structure and the measurements are inform of spatial resolution. (Stanbridge & Ewins 1999.) The figure 9 shows the measurement set-up using scanning vibrometer.



Figure 9. The measurement set-up showing the scanning laser Doppler vibrometer.

The modal analysis is possible using SLDV as it gives response to the excitation in a single output frequency. The process of getting the output response could be repeated to series of frequencies to obtain FRFs. The derivation of response data at discrete points prior to conducting modal analysis from sidebands of spectrums in SLDV is given by the following equation. (Stanbridge & Ewins 1999.)

$$v_z(t) = \sum \{V_{an} \cos(\omega t + \alpha_n) \cos^n \Omega t + V_{bn} \sin(\omega t + \alpha_n) \cos^n \Omega t\} \quad (17)$$

In equation 17, $v_z(t)$ is vibration velocity of a point in z-direction, V_{an} and V_{bn} are Fourier coefficients for the complex mode shape components and α_n is phase angle which can be derived from the magnitudes and phase angles at sideband frequencies. Ωt is the distance round the scan from the datum radius if circular measurement is taken. Stanbridge and Ewins (1999) have given the measurements procedure using SLDV where the rotating discs, straight lines scans, circular scans, and conical scans are described. (Stanbridge & Ewins 1999.) The displacement or velocity could be directly measured with the scanning vibrometer. The displacement demodulation gives better results in case of low frequency measurements whereas the velocity demodulation gives better results with higher frequencies. (PSV-500 2021.) For this thesis, the automated hammer is attached with the vibrometer to create an impulse to the system and manual hammer was used with accelerometer sensor.

2.6 Damping Ratios Using Half Power Method

The damping ratios are calculated using half power bandwidth method from the measured FRF. Figure 10 shows the half power bandwidth method (Krämer 1993). The half power points can be calculated using following equation 18.

$$\xi = \frac{\omega_2 - \omega_1}{\omega_n} \quad (18)$$

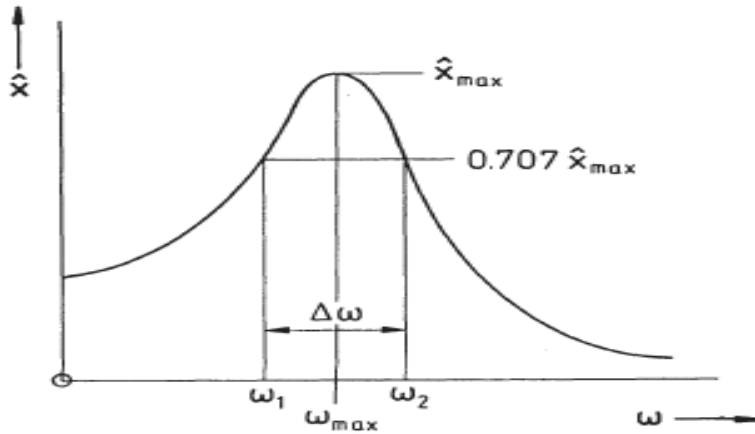


Figure 10. The half power bandwidth method for calculating damping ratios (Krämer 1993).

In equation 18, ω_n is modal frequency at a given amplitude peak of acquired FRF, ω_1 and ω_2 are the sidebands or half power frequencies, ω_n as shown in figure 11, which are obtained by multiplying the peak natural frequency by 0.707 and ζ is the damping ratio. There are other methods of extracting the damping ratios from the experiments.

2.7 Damping Ratio Using Logarithmic Decrement Method

The measurement of damping ratio can be determined by the rate of decay of the free oscillations such that the decay is larger if the damping is larger. The natural logarithm of two successive amplitudes can be termed as logarithmic decrement. (Thomson 1993, p. 33.) The logarithmic decrement can be applied as a decay rate of certain frequency given that the amplitude envelope is exponentially decayed. The equation for the logarithmic decrement δ is presented below and figure 11 shows the logarithmic decrement method (Inman 2014, p. 60).

$$\delta = \ln \frac{x(t)}{x(t+T)} \quad (19)$$

In equation 19, T is the period of oscillation and t_1 and t_2 in figure are the two successive amplitude peaks time. The relationship of the logarithmic decrement method to damping ratio ζ is given in the equation below. (Inman 2014, p. 60-61.)

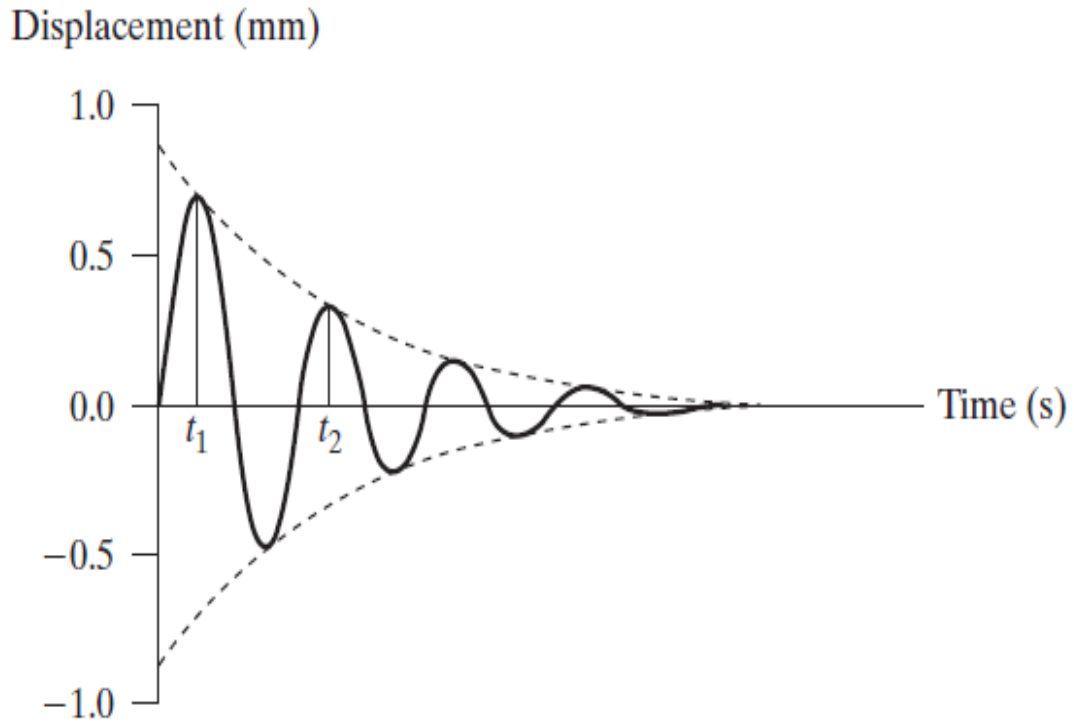


Figure 11. The logarithmic decrement to determine damping ratio (Inman 2014, p. 60).

$$\xi = \frac{\delta}{\sqrt{4\pi^2 + \delta^2}} \quad (20)$$

However, to increase the computational accuracy, any integer multiple of period could be used for measurement of the peak. For this, the logarithmic decrement equation can be as follows where, n is any integer number of successive peaks. (Inman 2014, p. 60-61.)

$$\delta = \frac{1}{n} \ln \frac{x(t)}{x(t + nT)} \quad (21)$$

There are other different methods used for computation of damping ratio from measurements such as Half-quadratic method, frequency response method, random decrement method, and so on. The damping ratio extraction methods and relationship is presented in figure in Appendix 1.

2.8 Numerical Simulation using MATLAB RoBeDyn Toolbox

The numerical simulation for this study has been done using Rotor Bearing Dynamics (RoBeDyn). The RoBeDyn toolbox was developed in Machine Dynamics Laboratory in LUT University, and it is in MATLAB environment. It is a finite element-based code pack that has been created to study the behavior of rotor dynamics system. RoBeDyn can be used to study the simple rotor bearing to more complex structures of the rotor systems. It can be used to calculate the free-free natural frequencies, damping ratios, and the mode shapes of the rotor. The frequency interference diagram (Campbell Diagram) for natural frequencies and damping ratios can be computed along with the mode shapes for any specific rotation speed needed. Steady state response due to unbalance forces and rotor dynamic instability can also be studied. RoBeDyn uses 12-Degree-of-freedom (DOF) beam FEM to model the flexibility of the rotor which is based on Timoshenko beam element. Mass elements is used to model mass of the disc and bearing was modelled as a spring damper. Along with other functions, the gyroscopic effects have also been incorporated into the analysis. The ball bearing properties needed in the study purpose of this thesis has also been incorporated within the RoBeDyn toolbox. (Sopanen 2019, p. 5.) The detail model for bearing and the modal reduction process have been explained in (Sopanen 2004).

2.8.1 Campbell Diagram

Campbell Diagram also known as Frequency Interference Diagram or Whirl Speed Map is a plotted graph of natural frequencies superimposed with forcing frequencies versus the shaft rotation speed. Speed dependent terms in the rotating machines such as gyroscopic matrix, stiffness and damping properties gives valuable information about the rotor dynamics analysis. (Sopanen 2019, p. 36.) It gives important information such as critical speeds and backward whirling (BW) modes and forward whirling (FW) modes.

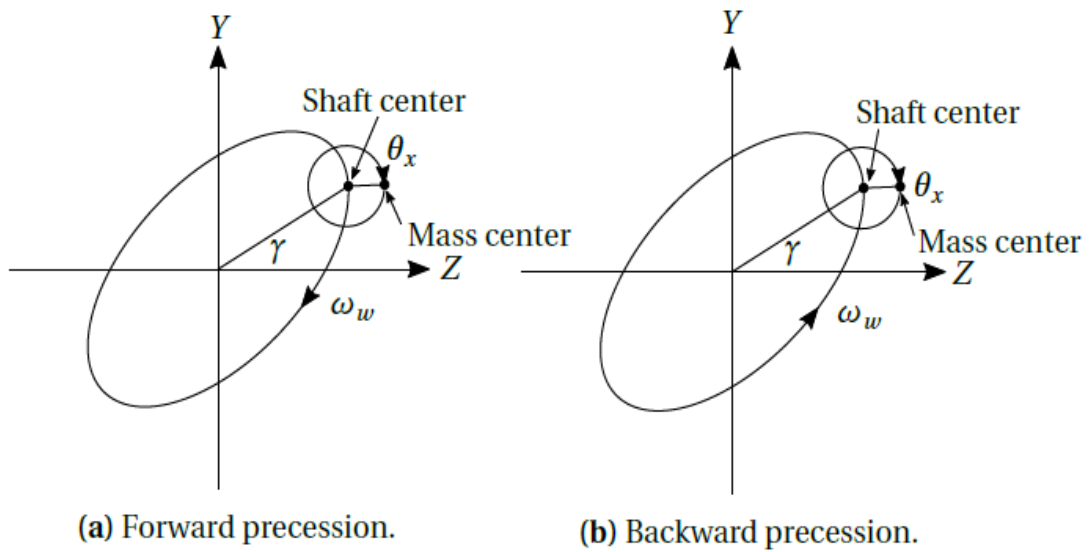


Figure 12. The rotor motion showing forward whirl and backward whirl (Sopanen 2019, p. 35).

Backward whirling in the rotor motion happens when the direction of whirl is opposite to the shaft spin speed whereas forward whirling happens if the whirling motion is in the same direction as the shaft spin. The figure 12 shows the forward and backward whirling phenomenon occurring during the rotor motion. (Sopanen 2019, p. 35.) The critical speed information achieved can be compared with the unbalance response plot to magnify the more accurate critical speed of the system.

3. Measurement

For experimental modal analysis of rotating rotor, the measurement was done based on a system where the rotor is supported by two bearings and the rotor has 3 discs. Verification of the model was done by employing three different methods of measurement. The rotor at rest was excited by a hammer and accelerometer sensor was used to get the modal parameters at first. Secondly, the rotor was driven at a specific frequency of 5 Hz and disc 3 at the free end of the rotor (right end) in below figure was excited using hammer. Thirdly, the measurement was taken by using the Scanning Laser Doppler Vibrometer (SLDV). The obtained results were analyzed and compared with the numerically simulated results in RoBeDyn. These methods will be discussed below in this chapter.

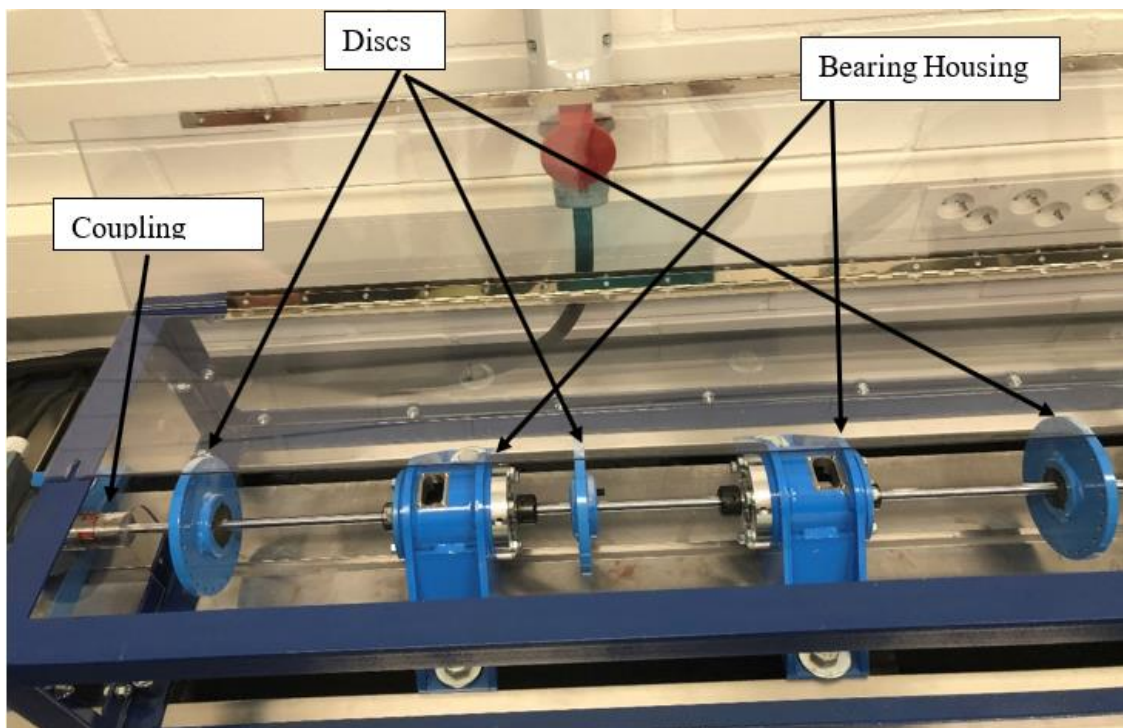


Figure 13. The test setup of rotor system in the LUT machine dynamics laboratory.

The figure 13 represents the test rotor configuration. The motor can be connected to the main rotor via ROTEX coupler. The coupling, discs and bearing housing are marked by the arrows.

3.1 Electric Motor

Thurm K21R 63 K 2 H motor by VEM motor has been used for the experiment with a power of 0.18 KW. The operation range for the motor used was from 0-2765 revolutions per minute (RPM). The rotor is connected to the motor by the ROTEX coupling by which the shaft of the rotor could be easily connected or disconnected to the motor. The parameters of the motor are presented below in table 3 and the parameters of ROTEX coupling is in table 4. (Parviainen 2019.)

Table 3. Motor Parameters (Parviainen 2019).

| | |
|--|---------------------------------------|
| Axle mass | 4.9 kg |
| Moment of inertia in xx-coordinate, J_{xx} | $1.3 \cdot 10^{-4}$ kg.m ² |
| Moment of inertia in yy-coordinate, J_{yy} | $5.0 \cdot 10^{-5}$ kg.m ² |
| Moment of inertia in zz-coordinate, J_{zz} | $5.0 \cdot 10^{-5}$ kg.m ² |
| Length of motor | 0.178 m |
| Diameter (Outer) | 0.118 m |
| Diameter (Inner) | 0 m |

Table 4. ROTEX coupling parameters (Parviainen 2019).

| | |
|--|---|
| mass | 0.135 kg |
| Moment of inertia in xx-coordinate, J_{xx} | $2.578 \cdot 10^{-5}$ kg.m ² |
| Moment of inertia in yy-coordinate, J_{yy} | $2.504 \cdot 10^{-5}$ kg.m ² |
| Moment of inertia in zz-coordinate, J_{zz} | $2.486 \cdot 10^{-5}$ kg.m ² |
| ROTEX Length | 0.064 m |
| ROTEX diameter (Outer) | 0.041 m |
| ROTEX diameter (Inner) | 0.012 m |

3.2 Bearings, Shaft and Discs

Two ball bearings are used in the setup. The used bearings are NSK 6007-ZZ type. The shaft used is made of structural steel rod. It has a length of 1 meter(m) and the diameter is 12 mm. The shaft has a material density of 7800 Kg/m^3 and the modulus of elasticity is $210 \cdot 10^{11} \text{ Pa}$. The disc properties are presented in table 5. (Parviainen 2019.)

Table 5. Disc Parameters (Parviainen 2019).

| | |
|--|--------------------------------------|
| Assembly mass | 1.69 kg |
| Moment of inertia in xx-coordinate, J_{xx} | $3.896 \cdot 10^{-3} \text{ kg.m}^2$ |
| Moment of inertia in yy-coordinate, J_{yy} | $1.991 \cdot 10^{-3} \text{ kg.m}^2$ |
| Moment of inertia in zz-coordinate, J_{zz} | $1.989 \cdot 10^{-3} \text{ kg.m}^2$ |
| Disc Length | 0.01 m |
| Diameter (Outer) | 0.150 m |
| Diameter (inner) | 0.012 m |

Three discs of identical properties are used for this work. The discs can incorporate 24 M6 bolts of mass $4.08 \cdot 10^{-3} \text{ kg}$ to create the unbalance on the system.

3.3 Measurement Sensors

The measurement was done with two different methods, SLDV and Accelerometer sensor. The accelerometer sensor using the Universal Serial Bus (USB) digital accelerometer type 333D01. The 333D01 accelerometer is based on piezoelectric crystal material which converts the mechanical signal to the voltage signals. The data can be easily recorded and read across mobile phones, tablet, or laptops. (Digiducer Inc. 2021a.) The data can be saved in MATLAB. The figure 14 shows the accelerometer sensor. The sensor has a magnetic mounting. The high frequencies signals can be affected because of the magnet interference with different materials in magnetic mounting types (Scheffer & Girdhar 2004, p. 34).

| | | |
|---|---------------------|--|
| Frequency Range ($\pm 10\%$) | 1.5 Hz to 11 000 Hz |  |
| Frequency Range ($\pm 3\text{dB}$) | 0.9 Hz to 15 000 Hz | |
| Frequency Range ($\pm 5\%$) | 2 Hz to 8 000 Hz | |

Figure 14. The operation range (bottom) used for measurement using 333D01 accelerometer sensor (left) and the accelerometer (right).

The sensor used was operated in the frequency range of 1.5 Hz to 11000 Hz and the sensitivity was 10% meaning that the sensor has flat response from 1.5 Hz to 11000 Hz within $\pm 10\%$ deviation from the calibrated sensitivity at reference frequency. 24-bit resolution was used for this purpose. For the specific frequency measurements, sampling rate of at least thrice the maximum expected frequency is advised and the use of 8000 Hz rate is advised to correctly measure the frequency of less than 20 Hz. There are two channels for measurement, channel A has a maximum frequency range of $\pm 196 \text{ m/s}^2$ and channel B has a maximum frequency range of $\pm 98 \text{ m/s}^2$. (Digiducer Inc. 2021b.)



Figure 15. The scanning head of SLDV taking the measurements.

For the used SLDV method, the PSV-500 scanning head with reference laser of OFV-505 was used. The PSV-500 can operate up-to 25 MHz frequency with the vibrational velocity of 0.01 micrometer per second to 30 meters per second. The OFV-505 sensor head integrates interferometer, Helium Neon laser with a maximum stand-off distance of 300 meters, and imaging optics in a stable housing. (PSV-500 2021.) The figure 15 shows the scanning head taking the measurements. The figure 16 below shows different components of the scanning vibrometer.

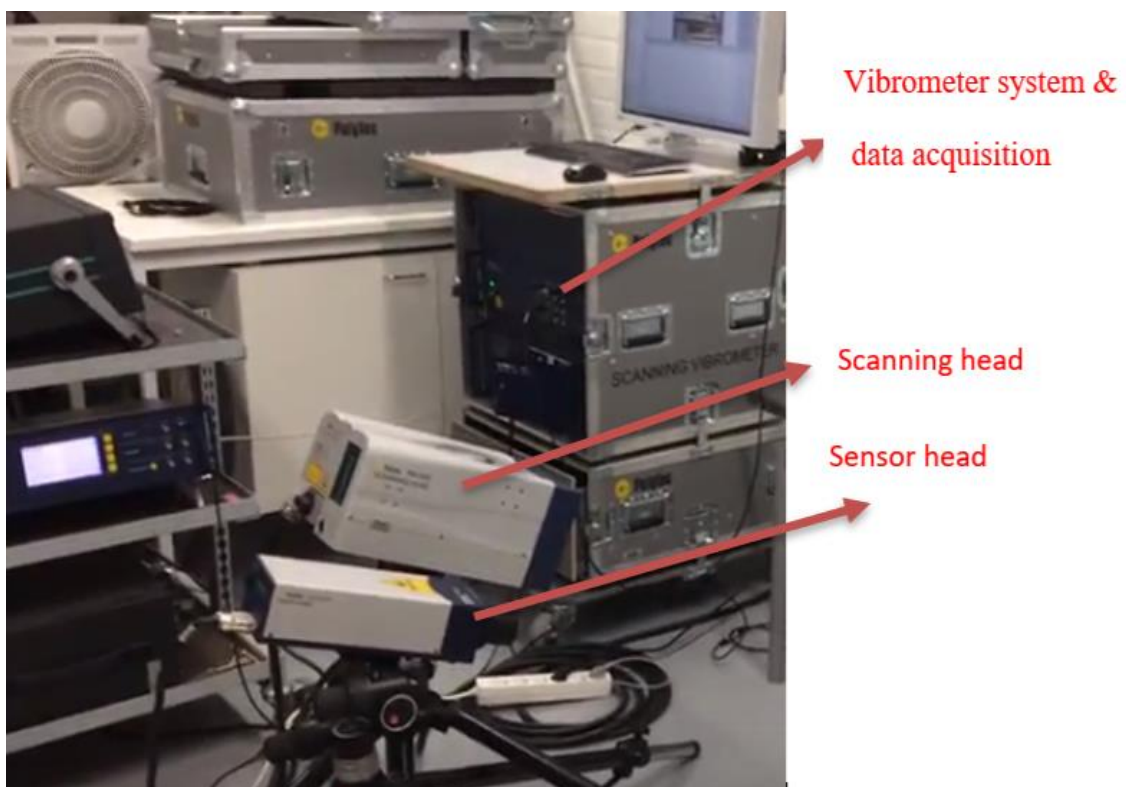


Figure 16. Different components used in the scanning vibrometer.

The scanning was done along the length of a rotor shaft by placing 9 measuring points which were sprayed with a reflective light to prevent the laser light from scattering. 3200 pixels resolution was used for measuring the frequencies from 0-100 Hz.

3.4 Measurement Set-up

For this project, the rotor system was arranged such that the motor was connected via ROTEX shaft coupler to the shaft of 1 meter length. The figure 17 shows the schematic of

experimental setup for the rotor system. The discs are colored as blue, and the bearings are orange. Nodes for the rotordynamics analysis are also shown. The numbers below are the distance from the coupling in centimeters.

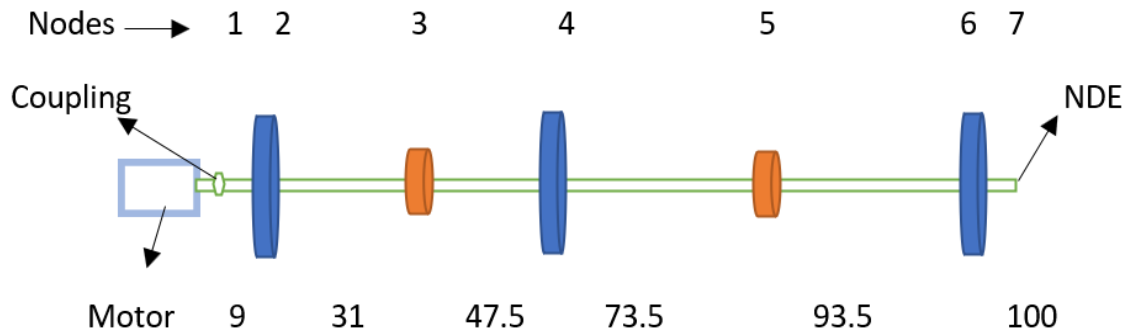


Figure 17. The rotor configuration.

The measurement was staged in 4 different ways.

- At first, the rotor at rest was excited by impact hammer at a fixed location of the rotor system and the frequency was taken by accelerometer sensor at different locations. Fixed location of the rotor was excited at disc 3 the measurement was taken from the shaft coupling, disc 3 and bearings.
- Secondly, the measurement of the frequency was taken from a rotating rotor with no external excitation at 5 Hz rotation frequency from the motor and the measurement were recorded for bearing 1 and bearing 2.
- Thirdly, the same rotation frequency of 5 Hz was applied to the rotor and the disc 3 was excited by the impact hammer. The recording for the frequencies were taken.
- After that, the Scanning Vibrometer was used to take the measurement of the stationary rotor system. The scanning vibrometer works in such a way that it utilizes the Doppler shift between the incident light and the scattered light travelling to the recording instrument to determine the velocity of a spot targeted by a focused laser beam. (Stanbridge & Ewins, 1999.) The damping ratios were calculated by using half power method from the obtained frequency response.

4. Results and Discussion

This section has been divided into case studies of the results for RoBeDyn, case studies for measurement with impact hammer excitation measured with accelerometer and case studies with the scanning vibrometer.

4.1 RoBeDyn Simulation Results

The wireframe plot for the rotor system to present the idea of the location of different components in the rotor system is presented in the figure 18. The FE model for RoBeDyn was designed such that there are 7 nodes and 6 elements. Discs are modelled as mass elements and bearing housing, couplings and damping properties are modelled as spring-damper elements. The material properties for rotor dynamic analysis in RoBeDyn has been presented in table 6 and the bearing parameters are presented next in table 7 (Parviainen 2019).

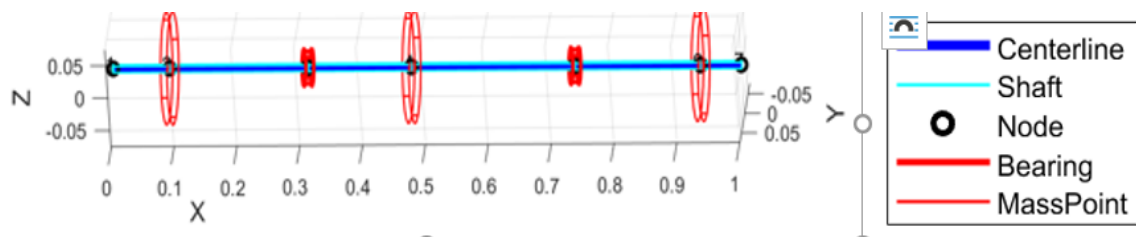


Figure 18. The wireframe plot of the RoBeDyn model showing the rotor system. There are 7 nodes and 6 elements.

The discs are located at node 2, node 4, and node 6 and bearing are located at node 3 and node 5. Free end on the left is DE at node 1 where coupling can be connected, and right end is free end of rotor at node 7.

Table 6. Material Properties of the rotor (Parviainen 2019).

| | |
|--------------------------|------------------------|
| Material Density, ρ | 7800 kg/m ³ |
| Poisson's ratio, ν | 0.3 |

| | |
|--------------------------------|------------------------|
| Modulus of Elasticity, E | $2.1 \cdot 10^{11}$ pa |
| Shear Correction factor, k_s | 0.8864 |

Table 7. Bearing Parameters (Parviainen 2019).

| Bearing Stiffness | Value |
|--|----------------------|
| Bearing Stiffness in Y-coordinate (K_{YY}) | $1.4 \cdot 10^8$ N/m |
| Bearing Stiffness at Z-coordinate (K_{ZZ}) | $1.4 \cdot 10^8$ N/m |

The damping in the rolling element bearings was computed using the equation,

$$cb = (0.25 \dots 2.5) \cdot 10^{-5} \cdot k \quad (22)$$

where, k is the linearized stiffness of the bearing (Sopanen 2004, p. 52).

4.2 The Campbell diagram and Unbalance Response

The result for RoBeDyn model presents the important information about the rotor's dynamic behavior. The Campbell diagram, which presents the critical speed information that is when the rotor spin speed matches one of the natural frequencies is a plot of the damped natural frequencies versus the rotor rotational speed (Chen & Gunter 2005, p. 60). Unbalance responses are also presented to know the vibration amplitudes versus the rotation speed. The motor was excluded for the RoBeDyn model, and the bearing was modelled as a spring damper with bearing stiffness of 1.4×10^8 for both Y and Z-directions. The damping ratios were put into the Inp.ModalDamping, which were derived from the measurement using half power method. The Campbell diagram of the rotor alone is presented in figure 19.

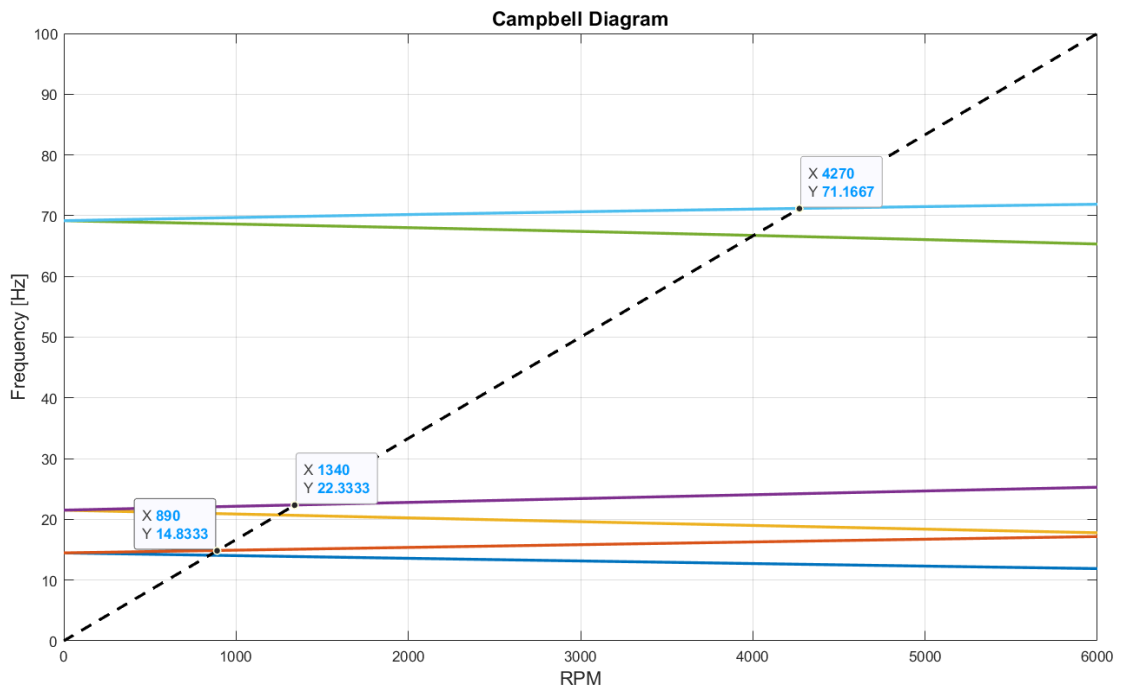


Figure 19. The Campbell diagram of the RoBeDyn model (rotor alone).

We see in the above Campbell diagram the forward modes frequencies are around 14.8 Hz, 22.333 Hz and 71.167 Hz. The backward modes frequencies are around 14 Hz, 20.5 Hz and 66.8 Hz. These were the modes computed constraining the displacement along X-axis and rotation about X-axis. The figure 20 shows the unbalance response plot.

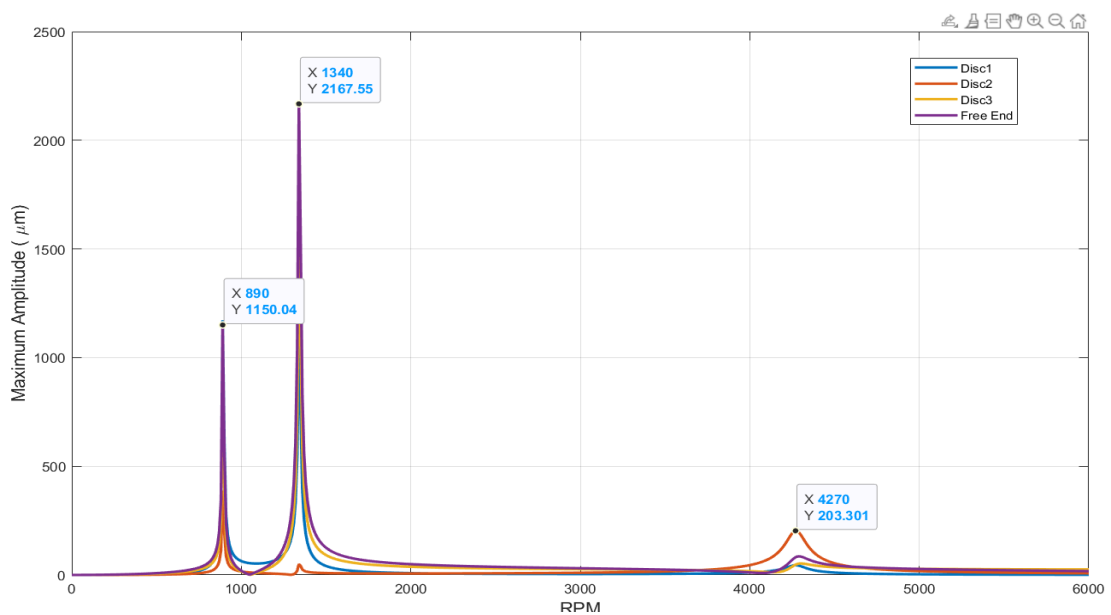


Figure 20. The unbalance response plot (rotor alone)

The figure above showing the unbalance response plot shows the three forward modes from Campbell diagram are matching with the unbalance response and thus those forward modes could be called critical frequencies. The rotor needs to avoid these critical frequencies to avoid the resonance phenomena. The unbalance response plot above is considered only for the discs and free end of the rotor because there was very minimal displacement in the two bearing locations. Since there was a critical frequency of 14.8 Hz not matching the done measurement, the modification was made such that the displacement in coupling side was constrained to check for an additional 14.8 Hz frequency. The figure 21 shows the Campbell diagram of the system after modification. The first forward mode we see is around 20 Hz and the first backward mode is around 18.7 Hz. The second forward mode was around 68.833 Hz, and the second backward mode was around 66 Hz. This shows the frequency of 14 Hz was mostly due to the coupling side.

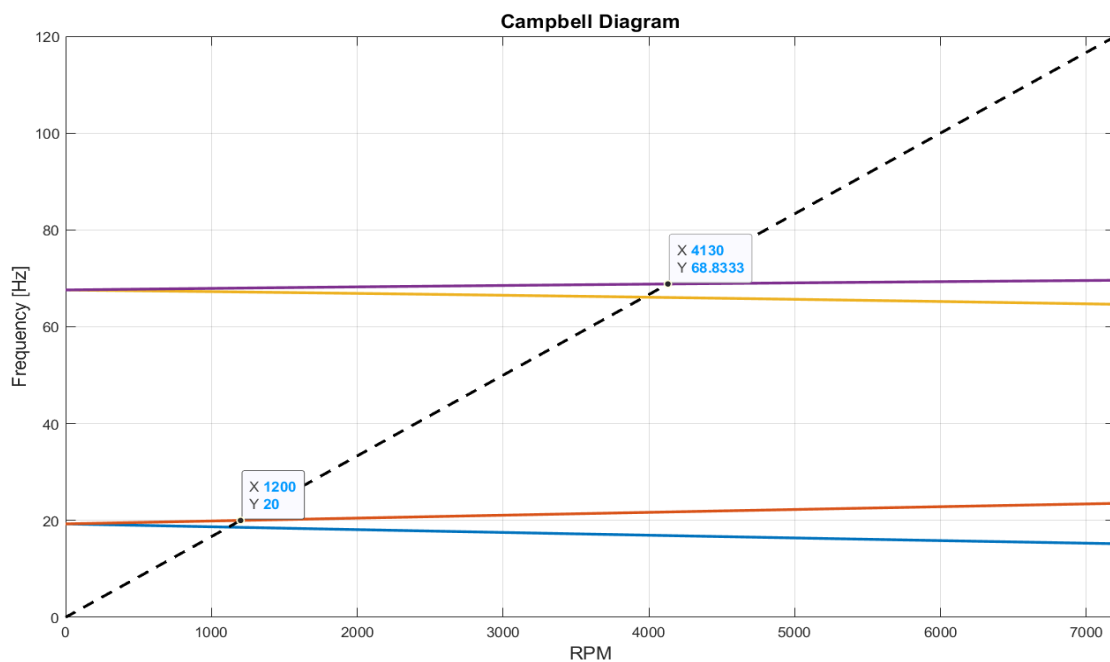


Figure 21. The Campbell Diagram, coupling side constrained (no displacement and no rotation).

The Campbell diagram in the figure 21 verifies that the coupling side was affecting the results. Unavailability of the realistic coupling data for the RoBeDyn analysis was the source of the additional forward and backward modes of 14.8 Hz and 14 Hz respectively in Campbell diagram of figure 19. The measured frequencies from done measurements (section

4.3 and section 4.4) of 23-26 Hz and 74 Hz were showing the deviation from the acquired Campbell diagram (figure 19) of less than 5 %.

There may be several reasons for the errors occurring in the RoBeDyn analysis. Firstly, the numerical simulation model is not a real model and hence, there can be some errors. In the RoBeDyn model, same material properties are used for all the components whereas in reality, the material properties of different components may be different. Thirdly, the added unbalance mass in the RoBeDyn was to create an unbalance in the system response. This might be different from the actual unbalance in the experimental components such as discs. Lastly, the bearing was modelled as a spring damper and the mass and damping of the bearing were not considered accurately in RoBeDyn model.

4.3 Case Study of Standstill Rotor with Impact Hammer and Acceleration Sensor

For this case, impact hammer was used to excite the disc 3 of the rotor system and the measurement of different locations on the rotor was taken from roving the accelerometer sensor. The measurement was done 3 times for each location and double tapping of the hammer was avoided to ensure the reliability, validity, and sensitivity aspects of the results. The figure 22 shows the hammer excitation horizontally at disc 3 and the accelerometer sensor placed at different locations in the rotor system for the measurement. The image on the left top of the figure shows the hammer excitation at disc 3 and measurement taken at coupling. The image on the top right is the hammer excitation at disc 2 and measurement taken at bearing 1. The image on the bottom left of the figure is the hammer excitation at disc 3 and the measurement taken at bearing 2. The bottom right image presents the hammer excited at disc 3 and measured at disc 3.

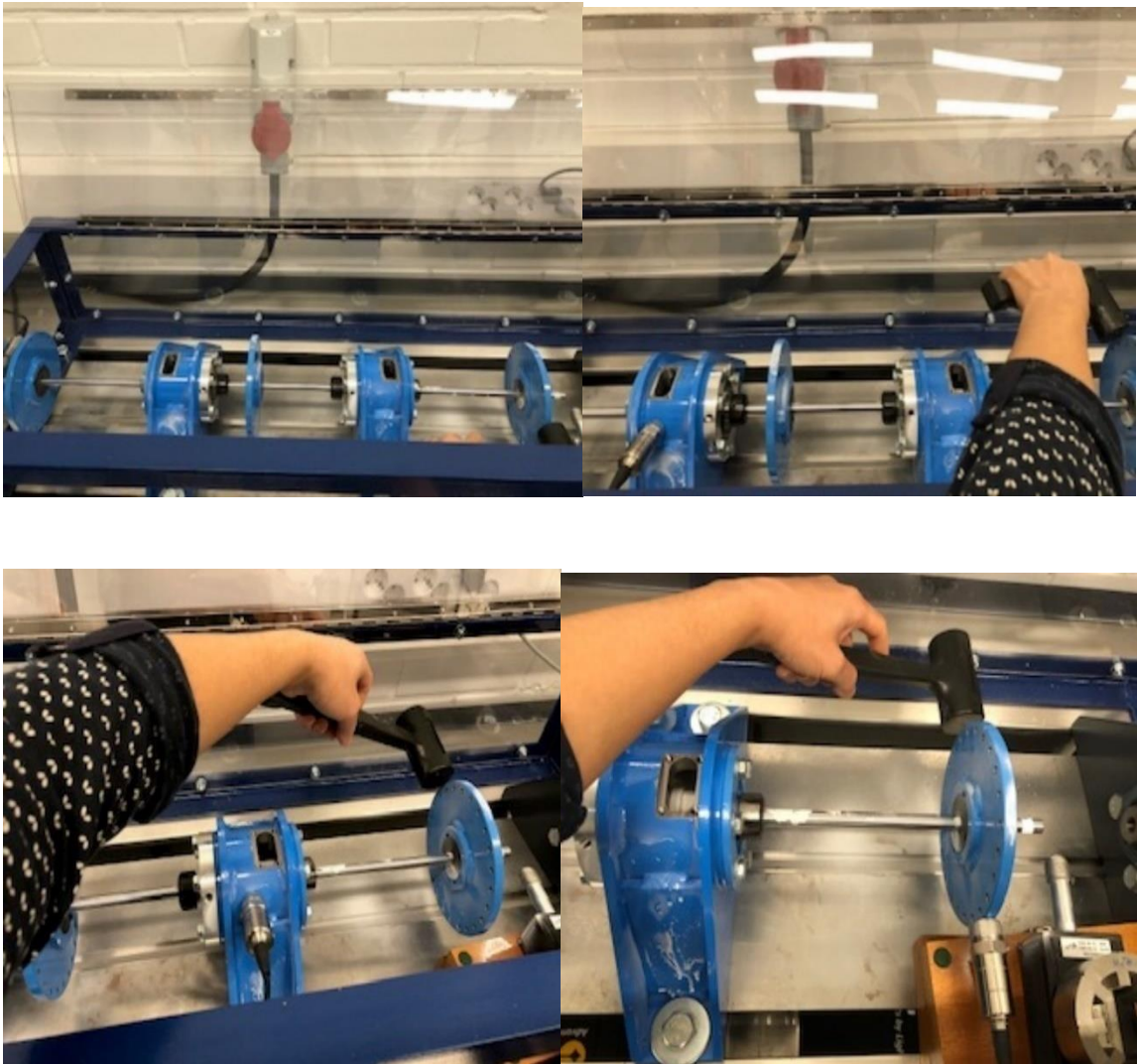


Figure 22. The hammer excitation and measurement taken at different locations of the rotor system.

Next, in the figure 23 presents the measured time signals and frequencies of the hammer excited disc 3 horizontally and measured by an accelerometer sensor at the coupling. In the figure above we see the two identical time domain hammer excitation and frequencies. This is due to the triaxial sensor used. the figures below also follow the same pattern. We see above that the first frequency is at 23 Hz. The second frequency is at 26.8 Hz. The higher frequencies are at 73 Hz and 103 Hz.

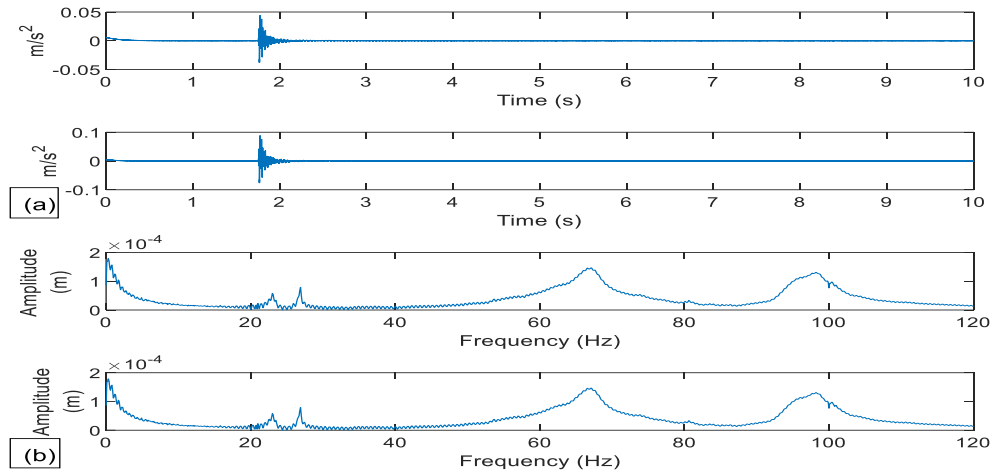


Figure 23. The measured responses at the coupling. (a) the time response with hammer excitation, X-axis is the time in seconds and Y-axis is the acceleration in m/s^2 and (b) the frequencies measured, X-axis is the frequency in Hz and Y-axis is the amplitude in meters.

We see the first two frequencies nearby each other is due to the horizontal and vertical stiffness of the bearing. The figure below shows the measurement taken at the first bearing housing. The figure 24 below shows the measurement taken at the bearing housing. We see the time domain image on the top and there are two frequencies nearby each other marked by arrows. The first frequency is at 23.4 Hz and the second frequency is at 26.8 Hz. These are also due to the horizontal and vertical stiffness of the bearing.

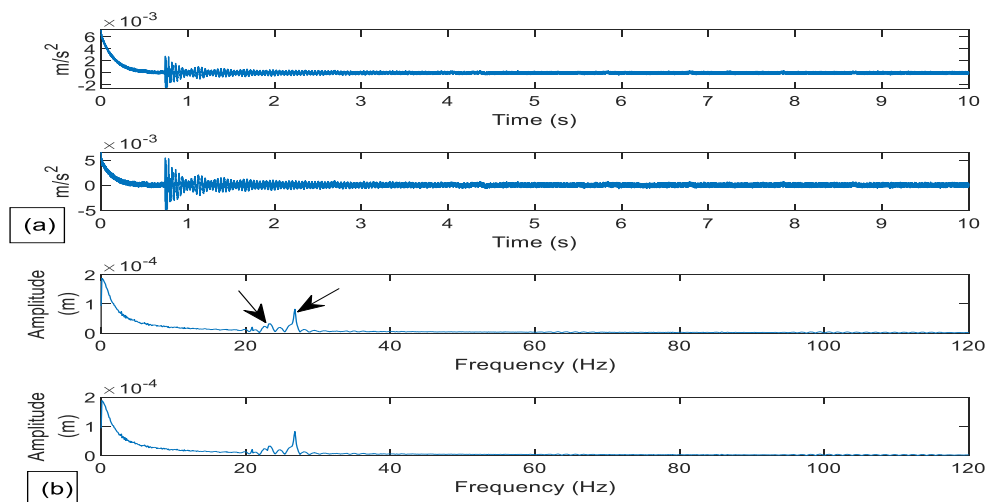


Figure 24. The measurement taken at first bearing housing. (a) is the time response from hammer excitation, X-axis is time in seconds and Y-axis is acceleration in m/s^2 . (b) the frequencies measured, X-axis is frequency in Hz and Y-axis is amplitude in meters.

Next, in the figure 25, we see the measurement taken at bearing housing 2.

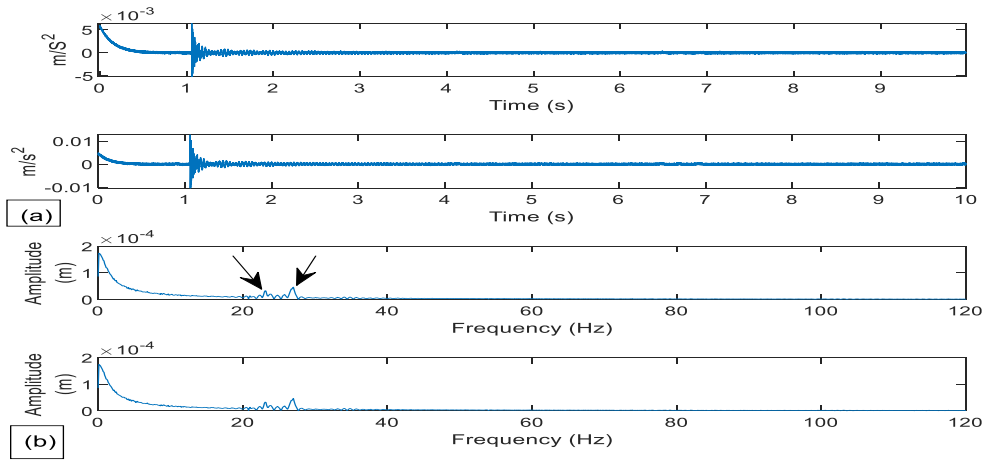


Figure 25. The measurement taken at bearing housing 2. (a) is the time response from hammer excitation, X-axis is time in seconds and Y-axis is acceleration in m/s^2 . (b) the frequencies measured, X-axis is frequency in Hz and Y-axis is amplitude in meters.

The measurement taken in the bearing housing two has similar frequencies peak like the measurement taken at the bearing housing 1. The first two frequencies are at 23 Hz and 26.9 Hz. These two nearby frequencies are the bearing stiffness in vertical and horizontal direction like in case of bearing 1 measurement. The figure 26 is for the measurement taken at the disc 3 and excitation also is on disc 3.

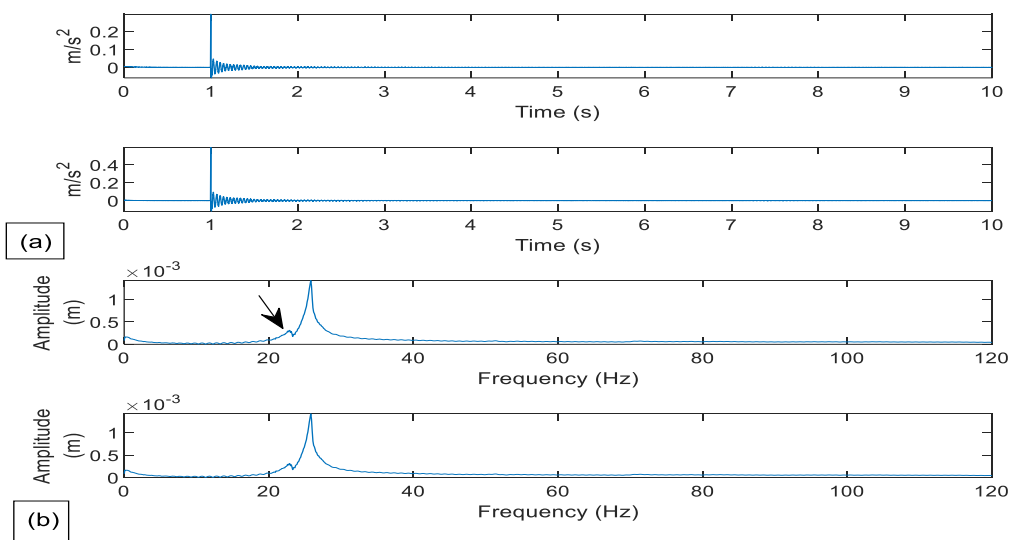


Figure 26. The measurement taken at disc 3. (a) is the time response from hammer excitation, X-axis is time in seconds and Y-axis is acceleration in m/s^2 . (b) the frequencies measured, X-axis is frequency in Hz and Y-axis is amplitude in meters.

In the above figure there is a bigger amplitude peak at 26 Hz. The small amplitude at 23 Hz is also seen but there is an overlapping of the amplitudes. However, as explained earlier these two nearby frequencies could be the result of the stiffness in vertical and horizontal stiffness of the bearings. Comparing different locations measurements, we can see that the overall modes shape in the rotor at around 26 and 27 Hz is bending frequencies near the disc 3 and free end of the rotor. This is obvious because of no support at those places. In the higher frequency in figure 23 where the measurement is taken in the coupling, there is a larger amplitude at 7 Hz frequency than measured at the bearing locations. This shows the bending modes shape in the coupling side.

4.4 Case Study of Rotating Rotor and Measurement with Accelerometer Sensor

The measurement for rotating rotor at a constant speed with 5 Hz frequency was done for this case. Initially, the rotor was rotated at 5 Hz frequency and the measurement were taken at bearing locations horizontally. After this, the hammer excited rotor at 5 Hz was measured in bearing housing 1 and then in bearing housing 2 by roving accelerometer sensor and the measurements were taken. The figure 27 shows the measurement taken at 5 Hz frequency with no external excitation at bearing housing 1.

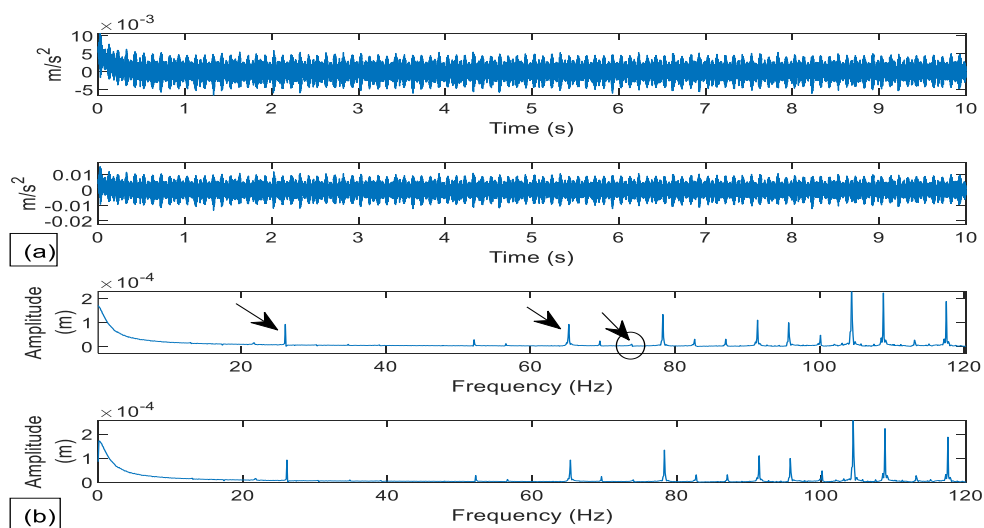


Figure 27. The measurement taken of spinning rotor at 5 Hz and sensor placed at the bearing housing 1. (a) is the time response from hammer excitation, X-axis is time in seconds and Y-axis is acceleration in m/s^2 . (b) the frequencies measured, X-axis is frequency in Hz and Y-axis is amplitude in meters.

In the figure above, the motor runs at a very low speed. The first peak at 26.1 Hz is like the standstill rotor case. The measurement data shows the shift in second frequency at 66 Hz, which is almost 8 Hz less than the standstill case. This could be the shift due to the forces developed and gyroscopic forces on the rotating rotor or could be the motor component frequency. However, the frequencies from the non-spinning rotor (section 4.3), the third amplitude peak was at 73 Hz and similarly in case of the spinning rotor shown above also have an amplitude around 74 Hz (marked by an arrow, inside the ellipse). The amplitude is about $1.019 \cdot 10^{-5}$ meters. There are other larger peaks after the measured peak at 74 Hz. Those frequencies after the 74 Hz frequency could be the bearing frequencies.

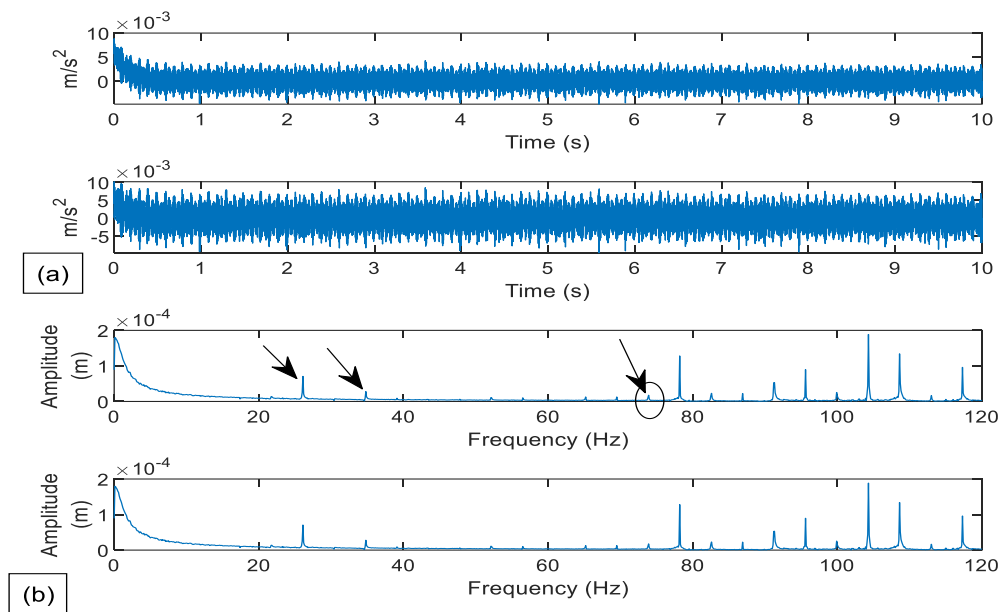


Figure 28. The measurement of spinning rotor and taken measurement from bearing 2. (a) is the time response from hammer excitation, X-axis is time in seconds and Y-axis is acceleration in m/s^2 . (b) the frequencies measured, X-axis is frequency in Hz and Y-axis is amplitude in meters.

In figure 28, we see the similar readings from the measurement as in figure 27 for the first frequency at 26.1 Hz but the second frequency is at 34.8 Hz. This frequency could be the motor component frequency. Similarly, the third frequency is at 73.9 Hz and this measured frequency marked by an ellipse and an arrow is also evident like in case of above figure and the standstill case.

The figure 29 shows the spinning rotor at 5 Hz excited by a hammer and measurement taken at the bearing 1 and the corresponding figure 30 shows the measurement taken at bearing 2 in a spinning rotor excited by a hammer.

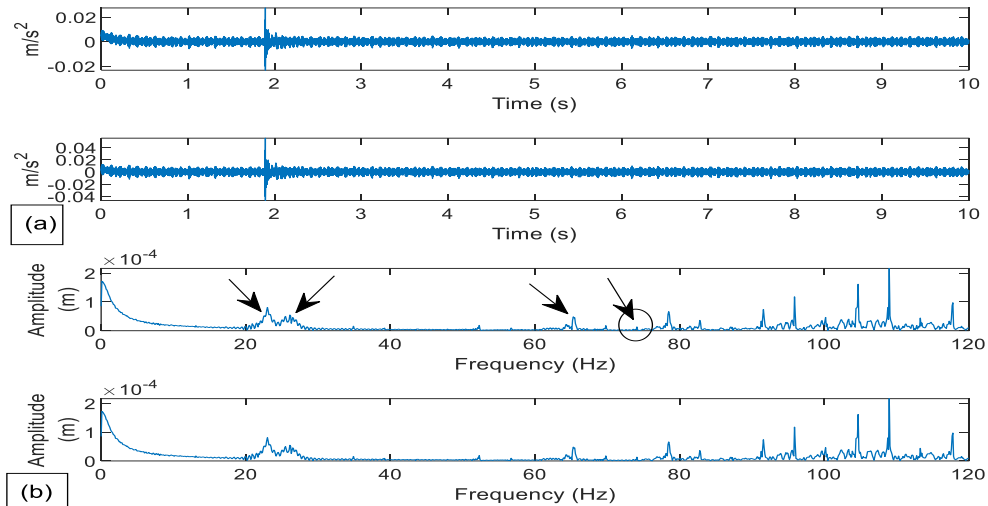


Figure 29. The measurement taken at bearing 1 and applied hammer excitation at disc 3. (a) is the time response from hammer excitation, X-axis is time in seconds and Y-axis is acceleration in m/s^2 . (b) the frequencies measured, X-axis is frequency in Hz and Y-axis is amplitude in meters.

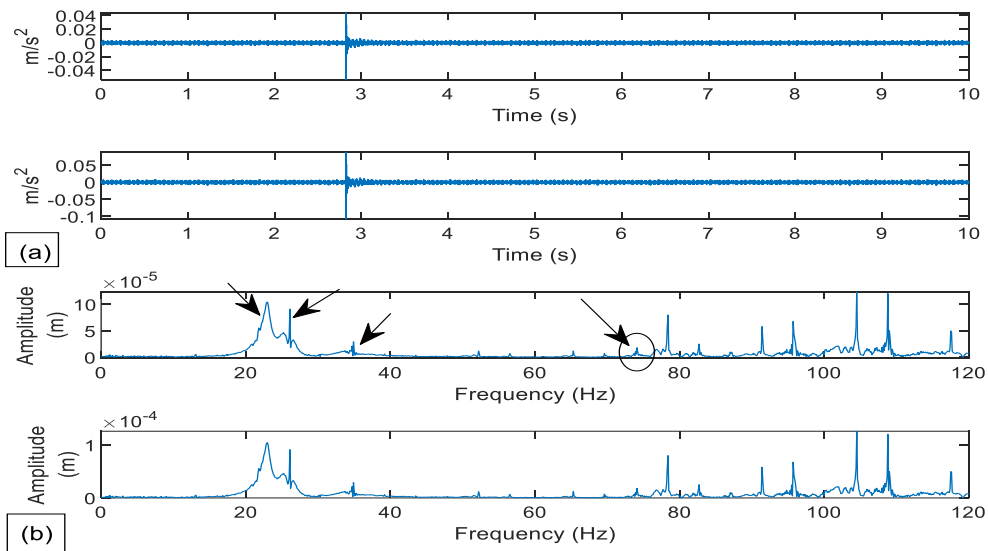


Figure 30. The measurement taken at bearing 2 and hammer excited on disc 3 for rotating rotor. (a) is the time response from hammer excitation, X-axis is time in seconds and Y-axis is acceleration in m/s^2 . (b) the frequencies measured, X-axis is frequency in Hz and Y-axis is amplitude in meters.

The figures 29 and 30 shows the measurement readings for the rotor rotating at 5 Hz excited by a hammer and the measurement taken at bearing housing 1 and bearing housing 2 respectively. For the measurement taken at the bearing 1 in figure 29, The first frequency is at 23.1 Hz and the second frequency is at 26.1 Hz. The first two frequency are however, overlapping with each other could be because of the horizontal and vertical stiffness of the bearing. So, considering just the 26.1 Hz frequency, it is matching with the stationary rotor case. The third amplitude peak occurs at 66 Hz which is like the rotating rotor with no external excitation measured at bearing 1 (figure 27) could be due to the motor components or due to the forces developed due to the rotation. In figure 30, the measurement taken at bearing 2 from the hammer excited rotor at 5 Hz speed, the first two frequencies are 23.1 Hz and 26.1 Hz and same as the earlier case measurements however, the third frequency is at 35 Hz like the case in figure 29 and could be either due to the forces developed due to rotating phenomena or could be the motor frequencies. There is also a small amplitude at 74 Hz (marked by an arrow and an ellipse) which is like the standstill case for both cases of hammer excited rotating rotors.

4.5 Case Study of Standstill Rotor with Scanning Vibrometer

Experimental modal analysis was also conducted using scanning vibrometer at the stationary condition of the rotor. The PSV-500 3D scanning head was used with OFV-505 reference laser. The automated hammer AS-1220 was used for exciting the rotor system with a square wave at a frequency of 0.2 Hz. The scattering of the laser beam on the reference laser was controlled by spraying reflective light over several measuring points across the rotor. 3200 pixels resolution was used. PSV 9.2 software was used to acquire the data and the data were recorded three times for each location point on the rotor to maximize the accuracy of the readings. The measured frequencies are presented in the figure 31 and figure 32.

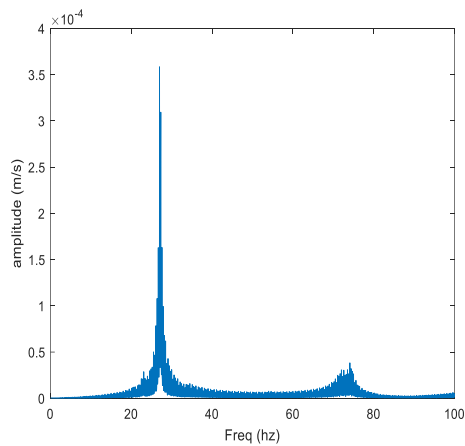


Figure 31. The acquired frequencies from the SLDV (left) and the first bending mode at 27.38 Hz (right).

The above figure 31, the frequencies obtained from the scanning vibrometer; the damping ratios were calculated using the half power bandwidth formulation as discussed in section 2.6. It is seen that the first bending mode at 27.38 Hz, the minimum displacement is at the bearing 1 followed by bearing 2 and the maximum deformation occurs near the disc 3.

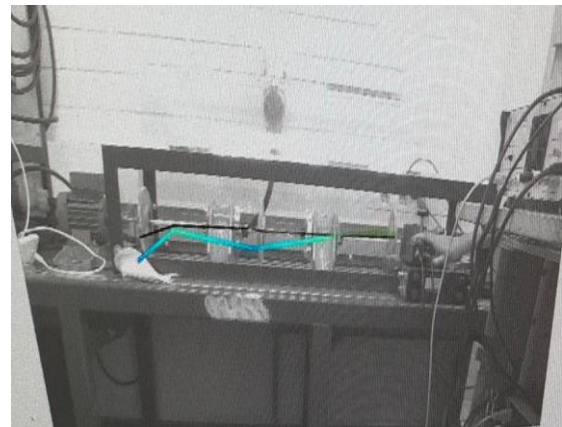
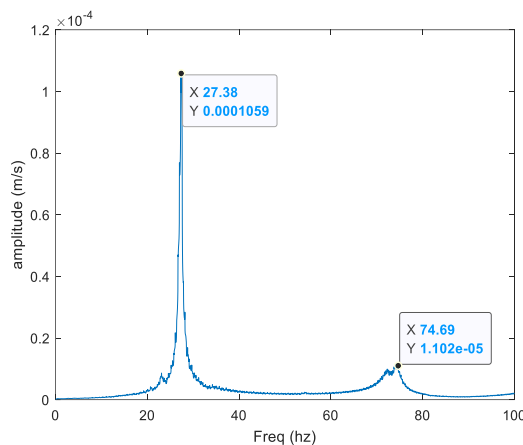


Figure 32. The refined acquired frequencies from the scanning vibrometer (left) and the second bending mode at 74.69 Hz (right)

The figure 32 above shows the refined frequencies after the half power calculation for damping ratios presented in equation 5 above. The obtained damping ratios were 0.0035, 0.0232, and 0.05. The second bending mode at 74.69 Hz, we see that the maximum deformation occurs near the disc 1 at the location around coupling.

4.6 Summary of the Obtained Results

Four different methods were used to obtain the frequencies and mode shapes for the rotor system. The first case was simulation. The second case was the hammer excited standstill rotors measured by accelerometer sensor at different locations of the rotor system. The third case was for the rotating rotor at 5 Hz frequency measured with the accelerometer sensor at the two bearings. Same rotation speed of 5 Hz was also applied for the hammer excitation and measurement taken at the two bearings by the accelerometer sensor. The final case was with the standstill rotor and measurement taken with the SLDV and automated hammer. The frequencies obtained from different methods are presented in table 8. Only forward modes frequencies from the simulation results are given for comparison and accelerometer sensor is represented by sensor.

Table 8. The frequencies obtained from different methods.

| Methods | Obtained Frequencies (Hz) | | | |
|---|---------------------------|------|------|-----|
| | | | | |
| Simulation | 14.8 | 22.3 | 71.2 | - |
| Sensor at coupling (standstill rotor + hammer) | 23 | 26.8 | 73 | 103 |
| Sensor at Bearing 1 (standstill rotor + hammer) | 23.4 | 26.8 | - | - |
| Sensor at Bearing 2 (standstill rotor + hammer) | 23 | 26.9 | - | - |
| Sensor at Disc 3 (standstill rotor + hammer) | 23 | 26 | | |
| Sensor at Bearing 1 (rotating 5 Hz) | 26.1 | 66 | 74 | 78 |
| Sensor at Bearing 2 (rotating 5 Hz) | 26.1 | 34.8 | 73.9 | 78 |
| Sensor at Bearing 1 (rotating 5 Hz + hammer) | 23.1 | 26.1 | 66 | 74 |
| Sensor at Bearing 2 (rotating 5 Hz + hammer) | 23.1 | 26.1 | 35 | 74 |
| SLDV (standstill rotor + automated hammer) | 27.4 | 74.7 | - | - |

For the measurement of the rotating rotors with or without impact excitation, there are some additional vibrational amplitudes observed. The higher frequencies beside mentioned in table 8 could be the bearing frequencies. The frequencies of around 23 Hz and 27 Hz are

found in almost each case of measurements and sometimes even with overlapping amplitudes. These frequencies could be due to the horizontal and vertical stiffness of the bearings and thus considered as a 26 Hz frequency as was in case of standstill rotor. In rotating case measured with or without excitation, we see the frequency of around 66 Hz when measured at bearing 1 and around 35 Hz when measured at bearing 2. These could be the shift either because of the additional forces developed and gyroscopic moments in the rotating rotor or could be due to the motor components or could be due to the bearing housing components. However, the speed dependent forces and gyroscopic moments (Friswell et al. 2010, p. 2) was very low but the shift was big in terms of measured frequencies. The cause behind this could be magnified if the rotor were run near the excited frequencies from the standstill case and the measurement were taken. However, from all the results the common bending frequencies obtained were in the range of 26-27 Hz and 73-74 Hz. Around 26-27 Hz maximum displacement was seen towards the disc 3 and the free end of the rotor meanwhile, the maximum displacement was observed near the coupling side at 73-74 Hz frequency.

5. Conclusions

The objectives of this thesis were to carry out experimental modal analysis of the rotating rotor. This has been achieved by measurement of the rotating rotor at 5 Hz speed and from FRF results it is evident that the measured response frequencies were not affected much by the additional forces in the rotating rotors and gyroscopic moments but if it was affected, it was a huge shift in terms of frequencies measured. However, those new frequencies in the rotating case compared to standstill case might be due to the motor components or bearing housing. If the response had small change as in case of repetitive similar frequencies measured as shown in table 8 in section 4.6, it might be due to the slow rotational speed applied as these forces are speed dependent (Friswell et al. 2010, p. 2) and these forces even if present might be negligible.

This thesis of experimental modal analysis of spinning rotor was commenced based on the literature findings from several authors. The experimental modal analysis was obtained by the equations presented in the chapter 2.2 of this thesis. The FRF (section 2.3) was obtained such that the harmonic force was applied to a location and the response in form of displacement was recorded from the sensor. The compliance (displacement/force) in the forms of amplitude peaks were treated as a SDOF response for the measured amplitude peaks of MDOF system such that each peak was bracketed as a single mode peak (Inman 2014, p. 588-589). Then, the damping ratio were calculated from each of the SDOF response peak by using Half Power bandwidth method in section 2.6. Impact hammer was used to excite the rotor system according to the section 2.4. The SLDV used was described in the section 2.5 with the equations for the rotating systems measurement by Stanbridge and Ewins (1999). The description of the sensors used for the measurement were also given in the section 3 and their properties were discussed for validating the results obtained.

The experimental modal analysis presented the vibration spectrum of the rotor bearing system. The obtained results were natural frequencies, mode shapes in form of relative displacement of the nodes and damping ratios from the measured natural frequencies by half power method. The obtained damping ratios from the modal analysis were modelled into the RoBeDyn toolbox for tuning the model. The motor and coupling were removed as it was noticed that the mass of the motor was significantly affecting the dynamic response of the

rotor system in the RoBeDyn modal analysis. The results obtained from RoBeDyn analysis was 5 % deviated from the measurement and the reasons are discussed in section 4.2 of this thesis.

The reliability, validity and sensitivity aspects for the measurement were achieved by first measurement of the rotor at rest and achieving the FRF with two different measurement process that is with SLDV and automated hammer, and with the accelerometer sensor and impact hammer. The results were compared and found that the results hold for both these measurement process. Also, the Measurement were taken three times for each location of the measurement to ensure the sensitivity of the result.

Conclusively, the measured modal parameters such as mode shapes, damping ratios, and frequencies agrees with both methods for measurement that is with accelerometer sensor and vibrometer. The frequency obtained for the rotor system was around 26-27 Hz and 73-74 Hz damping ratios obtained were 0.0035, 0.0232 and 0.05, and the mode shapes agreed to both methods.

Further research could be carried with shaker and magnetic bearing excitation for the same rotor bearing system. The RoBeDyn analysis could be done with more accuracy. The rotor speed could be manipulated for higher speed of 10 Hz, 15 Hz, 20 Hz and so on and compare the obtained FRFs to see the gyroscopic moments and additional forces developed by the rotational rotor effects. The operation range of the rotors could also be near the excited frequencies of the standstill rotor to evaluate the difference in the results obtained here.

References

Ahmed, H. & Nandi, A. K. 2019. Condition Monitoring with Vibration Signals. USA. IEEE press. John Wiley and Sons Ltd. 440 p.

Avitabile, P. 2001. Experimental Modal Analysis: A Simple Non-Mathematical Presentation. *Sound and Vibration*, 35:1. Pp. 20-31.

Bruel & Kjaer 2003. Experimental Modal Analysis: Sound and Vibration Measurement A/S. [Web Document]. [Referred 10.10.2021]. Available: <http://papai.modal.hu/prezentaciok/Br%C3%BCel%20and%20Kjaer.pdf>.

Bucher, I. & Ewins, D. J. 2001. Modal Analysis and Testing of Rotating Structures. *Philosophical Transactions of the Royal Society of London. Series A: Mathematical, Physical and Engineering Sciences*, 359:1778. Pp. 61-96.

Casiano, M. J. 2016. Extracting Damping Ratio from Dynamic Data and Numerical Solutions. Center for Aerospace Information (CASI). Hampton: NASA/Langley Research Center.

Cavalca, K. L., Cavalcante, P. F. & Okabe, E. P. 2005. An Investigation on the Influence of the Supporting Structure on the Dynamics of the Rotor System. *Mechanical Systems and Signal Processing*, 19:1. Pp. 157-174.

Cerna, M. & Harvey, A. F. 2000. The Fundamentals of FFT-Based Signal Analysis and Measurement. Application note-041 National instruments.

Chen, W. J. & Gunter, E. J. 2005. Introduction to Dynamics of Rotor-Bearing Systems. Victoria, Canada. Trafford Publishing. 469 p.

Chouksey, M., Dutt, J. K. & Modak, S. V. 2012. Modal Analysis of Rotor-Shaft System Under the Influence of Rotor-Shaft Material Damping and Fluid Film Forces. *Mechanism and Machine Theory*, 48:2012. Pp. 81-93.

Digiducer Inc 2021a. Digiducer Digital Ready USB Accelerometer. [Website] [Referred 10.11.2021] Available: <https://digiducer.digiducer.com/pages/faq-usb-digital-accelerometercom/pages/faq-usb-digital-accelerometer>.

Digiducer Inc 2021b. 333D01-Digiducer-T&M-Datasheet-(DS-0115). [Web Document] [Referred 27.10.2021] Available: [https://www.modalshop.com/filelibrary/333D01-Digiducer-T&M-Datasheet-\(DS-0115\).pdf](https://www.modalshop.com/filelibrary/333D01-Digiducer-T&M-Datasheet-(DS-0115).pdf).

Friswell, M. I., Penny, J. E. T., Garvey, S. D. & Lees, A. W. 2010. Dynamics of Rotating Machines. New York, USA. Cambridge University Press. 526 p.

Genta, G. 2005. Dynamics of Rotating Systems. New York, USA. Springer-Verlag. 658 p.

Gerhard, D. 2003. Audio Signal Classification: History and Current Techniques. University of Regina. Regina, Canada.

Gutierrez-Wing, E. S. 2003. Modal Analysis of Rotating Machinery Structures. Imperial College London (University of London). London, UK. Dissertation. 153 p.

Idehara, S. J. & Junior, M. D. 2020. Modal Analysis of Rotors with Whirling Motion Under Non-Stationary Conditions. Journal of Sound and Vibration, 481:2020. Pp. 115445.

Inman, D. J. 2014. Engineering Vibrations. USA. Pearson Education Inc. 707 p.

Jalali, M. H., Ghayour, M., Ziaei-Rad, S. & Shahriari, B. 2014. Dynamic Analysis of a High-Speed Rotor-Bearing System. Measurement, 53:07. Pp. 1-9.

Kärkkäinen, A. 2007. Dynamic Simulations of Rotors during Drop on Retainer Bearings. Lappeenranta. Lappeenranta-Lahti University of Technology. Dissertation. 91 p.

Krämer, E. 1993. Dynamics of Rotors and Foundations. eBook: Springer Science & Business Media. 383 p.

Kreuzinger-Janik, T. & Irretier, H. 2000. Experimental Modal Analysis—A Tool for Unbalance Identification of Rotating Machines. *International Journal of Rotating Machinery*, 6:1. Pp. 11-18.

Lee, C. 1991. A Complex Modal Testing Theory for Rotating Machinery. *Mechanical Systems and Signal Processing*, 5:2. Pp. 119-137.

Lee, C. & Joh, Y. 1993. Theory of Excitation Methods and Estimation of Frequency Response Functions in Complex Modal Testing of Rotating Machinery. *Mechanical Systems and Signal Processing*, 7:1. Pp. 57-74.

Lorenzo, E. D. 2017. Operational Modal Analysis for Rotating Machines: Challenges and Solutions. Leuven, Belgium. UNINA/FEDOA. Dissertation. 268 p.

Maierhofer, J., Gille, M., Thümmel, T. & Rixen, D. 2019. Using the Dynamics of Active Magnetic Bearings to Perform an Experimental Modal Analysis of a Rotor System. SIRM 2019- 13th International Conference on Dynamics of Rotating Machines. Copenhagen, Denmark.

Nordmann, R. 1984. Identification of Modal Parameters of an Elastic Rotor with Oil Film Bearings. *Journal of Vibration and Acoustics*, 106:1. Pp. 107-112.

Parviainen, T. 2019. Design and Simulation of Squeeze Film Dampers in Test Rig. Lappeenranta. Lappeenranta-Lahti University of Technology. Master's Thesis. 62 p.

Peeters, F., Pintelon, R., Schoukens, J., Rolain, Y., Gutierrez, E. S. & Guillaume, P. 2001. Identification of Rotor-Bearing Systems in the Frequency Domain part 1: Estimation of Frequency Response Functions. *Mechanical Systems and Signal Processing*, 15:4. Pp. 759-773.

PSV-500 2021. [Website] [Referred 09.11.2021] Available:
<https://www.polytec.com/eu/vibrometry/products/full-field-vibrometers/psv-500-scanning-vibrometer>.

Scheffer, C. & Girdhar, P. 2004. Practical Machinery Vibration Analysis and Predictive Maintenance. Jordan Hill, England. Elsevier Science. 255 p.

Sopanen, J. 2019. RoBeDyn V.2.2 Theory Manual. [Referred 10.09.2021] Lappeenranta: LUT Machine Dynamics. Not Available Publicly and Requires License.

Sopanen, J. 2004. Studies of Rotor Dynamics using a Multibody Simulation Approach. Lappeenranta. Lappeenranta-Lahti University of Technology. Dissertation. 91 p.

Stanbridge, A. B. & Ewins, D. J. 1999. Modal Testing Using a Scanning Laser Doppler Vibrometer. Mechanical Systems and Signal Processing, 13:2. Pp. 255-270.

Thomson, W. T. 1993. Theory of Vibration with Applications. eBook: CRC Press. 546 p.

Thorby, D. 2008. Structural Dynamics and Vibration in Practice: An Engineering Handbook. Oxford. Butterworth-Heinemann. 401 p.

Appendix 1

| Data Extraction Method | Damping Ratio Relationship | Notes |
|---|---|--|
| Half-power method | $\zeta \approx \frac{f_u - f_l}{2f_p}$ for $\zeta < 0.05$ | Convenient estimate from spectrum. Approximate for low damping ratio |
| Half-quadratic gain method | $\zeta = \sqrt{\frac{1}{2} - \sqrt{4 + 4\left(\frac{f_u - f_l}{f_p}\right)^2 - \left(\frac{f_u - f_l}{f_p}\right)^4}}^{-1}$ | Simple estimate from spectrum. Exact for force-excited SDOF response |
| General logarithmic decrement method | $\zeta = \frac{\ln(A_{t_1}/A_{t_2})}{\sqrt{(2\pi f_d \tau)^2 + \ln(A_{t_1}/A_{t_2})^2}}$ | For a linear exponential decay of an amplitude envelope. Exact for unforced SDOF decay |
| Power spectral density / autocorrelation method | Fitting method—see text | Used with PSD and autocorrelation and allows for function fitting |
| Frequency response method | Fitting method—see text | Used on complex FFT and allows for function fitting |
| Random decrement method | Fitting method—see text | Estimates a signal proportional to autocorrelation and allows for function fitting |
| Other Damping Ratio Relationships | | |
| Other Damping Ratio Relationships | Relationship | Notes |
| Complex frequency | $\zeta = \frac{f_i}{\sqrt{f_r^2 + f_i^2}}$ | Output from state-space models and finite element method models |
| Logarithmic decrement | $\zeta = \frac{\delta}{\sqrt{(2\pi)^2 + \delta^2}}$, where $\delta = \frac{1}{n} \ln(P_{t_1}/P_{t_n})$ | Traditional estimate. Evaluated by selecting successive peaks. Exact for unforced SDOF decay |
| Temporal absorption coefficient | $\zeta = \frac{\beta}{2\pi f_n}$ | Common estimate of physical models—appendix C |
| Spatial absorption coefficient | $\zeta = \frac{\alpha \cdot c}{2\pi f_n}$ | Classic characterization in acoustics and other branches of physics—appendix C |
| Quality factor | $\zeta = \frac{1}{2Q}$ | Classic figure of merit—appendix A |

Figure I The damping ratio extraction methods relationship (Casiano 2016).